Predicting Inflation with Recurrent Neural Networks

Livia Paranhos*

Bank of England

First version: November 2020

This version: September 2023

Abstract

This paper applies a recurrent neural network, the LSTM, to forecast inflation. This is an appealing model for time series as it processes each time step sequentially and explicitly learns dynamic dependencies. The paper also explores the dimension reduction capability of the model to uncover economically-meaningful factors that can explain the inflation process. Results from an exercise with US data indicate that the estimated neural nets present competitive, but not outstanding, performance against common benchmarks (including other machine learning models). The LSTM in particular is found to perform well at long horizons and during periods of heightened macroeconomic uncertainty. Interestingly, LSTM-implied factors present high correlation with business cycle indicators, informing on the usefulness of such signals as inflation predictors. The paper also sheds light on the impact of network initialization and architecture on forecast performance.

Keywords: inflation forecasting, machine learning, LSTM, dimension reduction.

*E-mail: Livia.Silva-Paranhos@bankofengland.co.uk. The views expressed are solely those of the author and do not represent the views of the Bank of England.

1 Introduction

A good forecast model for inflation is essential for economic agents and policy makers, yet up until recently, it was hard to improve over simple univariate specifications (Atkeson and Ohanian, 2001; Stock and Watson, 2007; Faust and Wright, 2013). New advances in machine learning have spurred the interest of economists in applying different methods to macroeconomic forecasting with the general promise of improvements in forecast accuracy. The common downside of machine learning techniques, including neural networks, is the lack of interpretability. For inflation prediction in particular this could be a problem, since much of the effort is devoted to understand the (likely unstable) underlying inflation process, sometimes at the expense of marginal increases in forecasting gains.

This paper investigates the ability of a special class of neural networks, the recurrent networks, to forecast inflation, and explores how these models can inform about the inflation process. While neural networks are well known by their flexibility in modelling complex data processes, recurrent networks were specifically designed to model sequences of observations, which makes them appealing for the study of time series. I consider specifically the LSTM (short for "long-short term memory"), a variation of the plain recurrent network, as the model of interest. This type of model differs from fully connected feed-forward networks in the way it handles past information. While the latter process all lags forwards (as its name suggests) and simultaneously in the network, recurrent models process each time step sequentially which enables the model to learn the dynamic dependencies in the data. LSTM networks in particular are able to learn from time steps far back in time, as opposed to plain recurrent models. In practice, this is achieved by incorporating a number of filters in the network that control the flow of information across time. This so called *long-memory* characteristic may be particularly important to model the long term trend of the series.

The paper also explores how the LSTM is useful as a nonlinear dimension reduction tool, which is in general achieved by carefully designing the network architecture (Goodfellow et al., 2016), to uncover economically-meaningful latent states that are behind the inflation process. The outcome can roughly be interpreted as a nonlinear generalization of common factors extracted from Principal Component Analysis (PCA). The difference is that, given the predictive nature of the model, the factors are in practice learned by supervision with the target variable, and should therefore carry information on the drivers of the inflation process.

I compare the forecasting performance of LSTM-based models with the fully connected feed-forward network (with varying input sets) and a number of benchmarks, including other machine learning models (Random Forest, LASSO, Ridge, and Elastic-net), as well as more traditional models in the inflation forecasting literature. I consider forecasting the US Consumer Prices Index (CPI) inflation, with extended results on Personal Consumption Expenditures (PCE) inflation in the Appendix.

RESULTS. On forecast performance, the estimated neural networks show competitive results against traditional benchmarks and other machine learning models, but these are not outstanding, in particular when compared to the random forest. The LSTM appears a good model to forecast at long horizons, which can be explained by its plausible ability in modelling long term trends, as well as during periods of instability, as it is relatively insulated from sudden, short-lived movements in inflation. Results for feed-forward models are more mixed, as these change with the horizon and input data, although their performance remains competitive against the benchmarks. Additionally, network architecture (here referring to the number of nodes in the network) is found to influence forecast performance. Smaller networks for which the number of nodes was *ex-ante* fixed show satisfactory, although generally worst, performance compared to bigger, cross-validated networks. This result encourages the use of ensemble techniques that account for multiple types of network architectures whenever the interest is mainly on forecast accuracy.

On inflation modelling, the LSTM reveals to be an interesting tool to reduce the dimensionality of the data in a way that is relevant for prediction. When estimated with the US FRED-MD database (McCracken and Ng, 2016), the estimated LSTM factors appear to capture well the underlying inflation trend and exhibit high correlation with business cycle indicators, in particular with the output gap, informing on the usefulness of such signals as inflation predictors themselves. Additionally, a variance decomposition analysis reveals that LSTM factors are significantly loaded on housing starts and corporate bond spreads, and they generally agree with the literature on common predictors of inflation.

In addition to make empirical contributions on the usefulness of these models for inflation modelling and forecasting, the paper also informs on more practical issues related to its implementation. In this respect, I discuss the impact of network initialization on forecast performance, as it is known that neural network predictions can be quite sensitive to initial conditions. According to a standard Diebold and Mariano (1995)-type statistic, I show that the ensemble prediction—the average prediction of models embedding different initial values—is at least as good as the prediction

of networks with a specific initialization, a result that is reassuring given the widespread use of this technique for this class of models. Additionally, the exercise also reveals that predictions from networks with different initial values are highly heterogeneous, which suggests that in practice the algorithm usually gets stuck into local optima, which again supports the use of ensembles.

RELATED WORK. This paper relates more broadly to the literature on inflation forecasting, and more specifically to papers applying neural networks to inflation or macroeconomic forecasting. The paper also relates to the vast literature on dimensional reduction techniques, where here I discuss the narrower literature on the use of deep neural nets for this purpose.

The conventional literature on inflation forecasting usually refers to Phillips curve-based models that relate inflation to some activity variable and autoregressive terms (Stock and Watson, 2009 provide an overview). Although well-established, forecasts based on the (more traditional) Phillips curve have varying performances over time and can be quickly overperformed by univariate models, as the random walk (Atkeson and Ohanian, 2001), the unobserved components model (Stock and Watson, 2007), or autoregressive models more generally. Other commonly used benchmarks are the Bayesian vector autoregression model (Giannone et al., 2015) and dynamic factor models (Stock and Watson, 2002; Ludvigson and Ng, 2007).

The recent improvements in machine learning have shifted the attention of econometricians to new, promising techniques for macroeconomic forecasting (Exterkate et al., 2016; Chakraborty and Joseph, 2017; Medeiros et al., 2019; Coulombe et al., 2020).[1] For instance, in an extensive exercise to forecast US CPI inflation, Medeiros et al. (2019) point to large improvements in forecast accuracy of machine learning models incorporating a large pool of predictors, especially the random forest model. The forecasting exercise of the present paper is roughly similar to theirs in terms of sample, data and the benchmark models considered (although their paper is more extensive on this), the difference being that here I extend the analysis to neural networks and recurrent networks in particular.

Regarding the specific use of neural networks for inflation and macroeconomic prediction, this paper is part of a modest yet growing literature. Early papers are e.g. Kuan and White (1994), Nakamura (2005) and McAdam and McNelis (2005). With the advances in computing power and big data, this literature grew, with examples considering feed-forward neural networks (Choudhary and Haider, 2012; Chakraborty and Joseph, 2017; Coulombe, 2022), plain recurrent

[1] In the field of economics more broadly, see for example Mullainathan and Spiess (2017) and Athey (2019) for an assessment of those methods applied to policy analysis and causal inference respectively, Varian (2014) for a discussion about big data in economics, and Refenes and White (1998) and Gu et al. (2019) for applications in finance.

neural networks (Sermpinis et al., 2014), and LSTM networks (Cook and Hall, 2017; Almosova and Andresen, 2019; Verstyuk, 2020). On LSTM networks in particular, Cook and Hall (2017) compare the forecasting performance of different network models, including a deep neural network, a convolutional network, the LSTM, and an encoder-decoder network, in a univariate exercise for US unemployment. Verstyuk (2020) compares a small-scale LSTM model to vector autoregression specifications in terms of forecasting accuracy and impulse response dynamics. Almosova and Andresen (2019) is the paper that most resembles the present one. The authors compare the forecasting performance of the LSTM with a feed-forward network and linear benchmarks in an exercise with US CPI. In terms of accuracy, they also point to a better performance of the LSTM at long horizons and highlight the importance of network architecture on the results. One difference is that they consider a univariate framework, while the present paper explores the use of big data and dimensional reduction. Additionally, this paper presents a wider set of benchmark models which includes other widely applied machine learning models, as the random forest and shrinkage methods.

Finally, this paper also touches the field of dimension reduction. In addition to prediction tasks, deep learning is also an interesting tool for nonlinear compression and can be regarded as a generalization of PCA (Hinton and Salakhutdinov, 2006). The use of this technique has been growing recently, with applications using Encoder-Decoder structures in an unsupervised fashion (Andreini et al., 2020; Hauzenberger et al., 2022), or in a supervised, forecasting framework (Coulombe, 2022). This work relates more closely in this regard to Coulombe (2022). The author uses a carefully designed deep neural net to extract *ex-ante* unobserved components of the Phillips curve in a supervised exercise to forecast inflation. The present paper does not impose the linear structure inherent to the Phillips curve as in Coulombe (2022), and extracts economically-interpretable factors via a careful selection of predictor sets. It is worth mentioning the relation between the LSTM and Encoder-Decoder models as dimension reduction tools. In the latter, the encoder is responsible for compressing the original data into a generally small number of components (the factors) and the decoder for relating these factors to the target (in the case of Autoencoders, the target would be the original data itself). The LSTM model applied in this paper can be seen as a variant of this type of model, where a first block containing the LSTM structure plays the role of the encoder (as it maps the original data into a low-dimensional state), and a second block involving a deep feed-forward network operates as the decoder, linking the information from the factors to the target variable. Although it is not *ex-ante* clear what are the

differences between the implied factors of each method, it is likely that LSTM factors give more emphasis to dynamic dependencies in the data and less to other forms of nonlinearities arising between predictors, and that Encoder-Decoder factors are better suited to capture these type of nonlinearities as per the deep network structure of the encoder.

OUTLINE. The organization of the paper is as follows. Section 2 introduces the econometric framework and the neural network models. Section 3 discusses model selection while Section 4 presents the data. Section 5 investigates the properties of the estimated LSTM factors. Section 6 discusses out-of-sample forecast performance, and Section 7 the sensitivity analysis over network initialization. Section 8 concludes.

2 Econometric framework

Consider the set of macroeconomic predictors $\mathcal{Z} = (w_t, z_t)'$, where w_t is a vector collecting the inflation series to be forecast as well as disaggregate inflation components, and z_t is a vector collecting macroeconomic series excluding w_t. Importantly, the set w_t is not contained in z_t, which allows me to isolate the predictive effect of the macroeconomic variables on inflation. Without loss of generality, I set the first element of w_t as the inflation series to be forecast, and denote it by y_t.

Let x_t be the NL-size vector collecting the predictors at time t and their lags. In this paper, I consider predictor sets of the form $x_t = (z_t, ..., z_{t-(L-1)})'$, $x_t = (w_t, ..., w_{t-(L-1)})'$ or $x_t = (z_t, ..., z_{t-(L-1)}, w_t, ..., w_{t-(L-1)})'$, where N changes accordingly across sets. I assume that the h-step ahead inflation y_{t+h} evolves nonlinearly with respect to the predictors x_t through the function G, such that

$$y_{t+h} = G(x_t; \Theta_h) + \varepsilon_{t+h}. \tag{1}$$

Θ_h collects the model parameters and ε_{t+h} is the prediction error. The underlying statistical problem consists therefore in estimating the unknown function $G : x_t \mapsto y_{t+h}$.

In this application, G takes the form of a neural network, in which case fitting the function to the data corresponds to estimating Θ_h given a network architecture. An architecture $\mathcal{A}_G$ is specified as being a collection of choices that defines the functional form of G. It embeds two elements, (i) the neural network model (or a combination of neural network models), and (ii) hyperparameters specific to the model. The network models considered in this paper are the feed-forward network, the recurrent network with LSTM units—referred here as the LSTM model—, and a combination of both, the FF-LSTM, as detailed below. Importantly, the choice

of the network is defined *ex-ante* by the researcher while the hyperparameters are selected via cross-validation. Making an analogy to the nonparametric literature, the hyperparameters can be viewed as tuning parameters that are model-specific, e.g. the bandwidth in kernel regression, or the choice of k in k-nearest-neighbors estimation.

Let $\mathcal{S}_{\mathcal{A}_G}$ be the set of parameters specific to architecture $\mathcal{A}_G$. The parameters $\Theta_h \in \mathcal{S}_{\mathcal{A}_G}$ are estimated by minimizing the mean squared error loss

$$\hat{\Theta}_h = \underset{\Theta_h \in \mathcal{S}_{\mathcal{A}_G}}{argmin} \left\{ \frac{1}{T-h} \sum_{t=1}^{T-h} \Big(y_{t+h} - G(x_t; \Theta_h) \Big)^2 \right\} \tag{2}$$

for a given set of predictors x_t and target variable y_{t+h}, where the estimation is implemented by gradient descent (more details in Appendix C).

The next sections present a detailed description of the three models considered. They mainly differ from one another with respect to the underlying network structure and the predictor set.

2.1 The feed-forward model

This is the plain fully connected feed-forward (FF) network. It consists of a potentially large number of simple elements (nodes) that are organized into layers: (i) a first layer that receives the raw input information, (ii) a final layer that corresponds to the network predictions, and (iii) hidden layers that lie in between, processing information in one direction, from the first to the last layer. Figure 1 provides a schematic representation. Each node in a given layer receives a linear combination of the outputs a from the previous layer in the network, $a'w + b$, where w and b are parameters, and returns a nonlinear transformation of it, $\sigma(a'w + b)$. The estimation of the model consists of learning the parameters in the network, also known as weights, using gradient descent (details in Appendix C).

I consider using the rectified linear unit (ReLu), $z \mapsto max\{0, z\}$, as the nonlinear transformation applied at each node, following modern practices in deep learning. Recent works on deep neural networks (networks with a large number hidden layers) establish formal results on the statistical properties of ReLu-based networks and derive faster rates of convergence compared to networks using sigmoid-based functions (Schmidt-Hieber, 2020; Farrell et al., 2021). These works follow the enormous success of ReLu-based deep nets in prediction tasks which are now becoming the state of the art in many contexts.

More formally, consider a feed-forward neural network with $q + 1$ layers in total. Let a_i be the

Figure 1: The feed-forward neural network

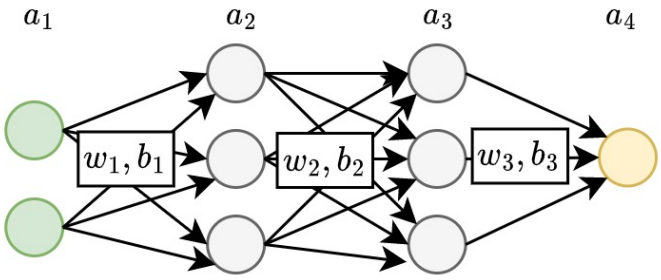

Schematic representation of a feed-forward neural network with $q + 1 = 4$ layers, $n = 3$ nodes per hidden layer, 2 inputs and 1 output.

hidden layer containing n nodes, for $i = 2, ..., q$.[2] The feed-forward model takes the form

$$\begin{aligned} g_{FF}(x_t) &= w_q' a_q + b_q \\ a_i &= ReLu(w_{i-1}' a_{i-1} + b_{i-1}), \quad i = 2, ..., q \\ a_1 &= x_t, \end{aligned} \tag{3}$$

where $\{w_i, b_i\}_{i=1}^{q}$ are the parameters of the model. Hence for the FF model, $G(x_t; \Theta_h) = g_{FF}(x_t)$. The dimension of each parameter depends on the layers it connects. Specifically, $w_1 \in \mathbb{R}^{NL \times n}$, $\{w_i\}_{i=2}^{q-1} \in \mathbb{R}^{n \times n}$, and $w_q \in \mathbb{R}^{n \times 1}$, while for the intercept terms, $\{b_i\}_{i=1}^{q-1} \in \mathbb{R}^{n \times 1}$ and b_q is a scalar. The hyperparameters of this model are the number of layers q, the number of nodes per layer n and the number of lags L to include in the input vector x_t. Note here that the size of the output layer is fixed to one given the single-valued target variable.

I consider estimating this model with both inflation-only data, $x_t = (w_t, ..., w_{t-(L-1)})'$, as well as with the pool of economic predictors, $x_t = (z_t, ..., z_{t-(L-1)})'$. The first case, called FF-cpi, is a natural nonlinear extension of the autoregressive model that maps lags of inflation (and its components) to the h-step ahead inflation. The second case, called FF-pool, forecasts inflation with a large set of macroeconomic predictors (and its lags). The total number of parameters of the feed-forward model is $(NL + 1)n + (Q - 1)(n + 1)n + (n + 1)$.

[2]The restriction that each layer must contain the same n number of nodes is imposed for simplification.

2.2 The LSTM model

The LSTM is a variant of the recurrent neural network. This type of model differs from FF networks in the way it handles past information. While FF models process all the input lags forwards and simultaneously in the network, recurrent networks process each time step sequentially, allowing the output of a previous time step to be the input of the following one. Note that in this case the information flows across the lag structure of the data, while in FF models it essentially flows across layers where the dynamic structure is not explored explicitly. This feature makes recurrent neural nets quite attractive to model time series, as they "remember" the information contained in previous time steps and may use it to improve prediction accuracy.

The main insight from the recurrent structure is a so called *internal memory* that is updated at each time step. The model then estimates the parameters such that its internal memory embeds the relevant information to forecast the target, but importantly it does so by taking into account the sequential dependency inherent in the data. For example, if low inflation is associated with a low output gap that persists during a period of time, but not with a low output gap that is essentially transitory, then the model is in principle able to learn these dynamic dependencies and extrapolates it to the forecast. An additional interesting feature of these models is their ability to generate factor-like estimates that are relevant for predicting inflation. This property is alike as the supervised nature of partial least squares as an alternative to principal component regression, which is by definition unsupervised. This essentially follows from the fact that the parameters of the LSTM model are learned by supervision with inflation, and consequently the components of the internal memory as well. In the rest of the paper, I interpret and refer to the internal memory as *LSTM factors* in an analogy to factor analysis.

To be more concrete, consider e.g. the predictor set $x_t = (z_t, ..., z_{t-(L-1)})'$ collecting the $N \times 1$ vector of predictors and their lags. The LSTM factors are represented as a p-vector denoted f_t and are a function of both the current input information z_t and the lagged factors f_{t-1}. Importantly, this recursion is limited to a fixed lag L in a way that past information can only be traced back up to L. In order to embed this idea in the notation, I write $f_{t|L} \equiv f_{t|t,t-1,...,t-(L-1)}$. In practice, the recursion behind the LSTM takes into account an additional component (the "cell state" in machine learning jargon) that ensures that the algorithm is able to learn from time steps far away in the past. This is in contrast to a plain recurrent neural net that suffers form vanishing gradients (more details on plain recurrent nets are in Appendix B). The ultimate structure of the LSTM

Figure 2: The LSTM and the flow of information

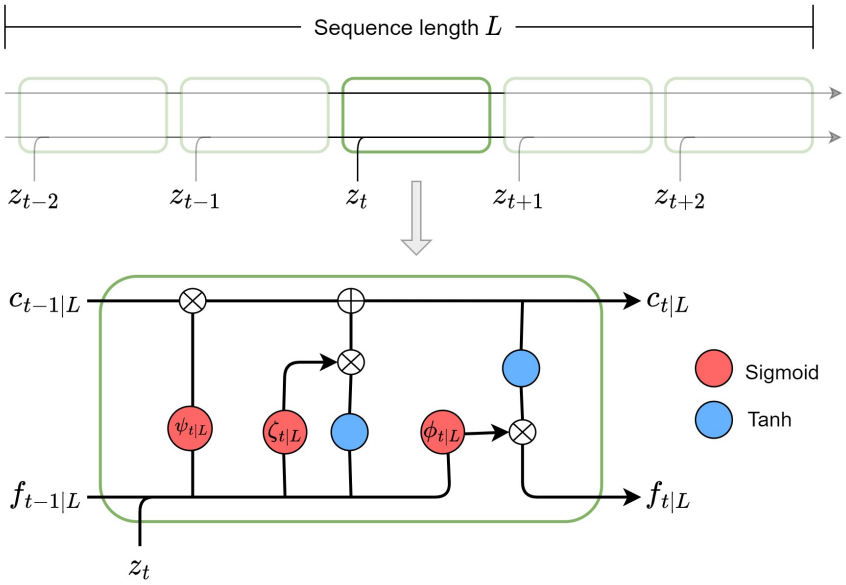

The figure is a visual representation of the LSTM equations in (4). Symbols $\oplus$ and $\otimes$ denote element-wise addition and multiplication respectively.

then combines the cell state, denoted $c_{t|L}$, with the LSTM factors $f_{t|L}$ through a number of filters $(\psi_{t|L}, \phi_{t|L}, \zeta_{t|L})$ that essentially control the flow of information through time. These filters are defined as sigmoid functions that are themselves learned from the data. The hyperbolic tangent (tanh) is also used in the model to squeeze the information between $[-1, 1]$ whenever additive structures are present. Figure 2 gives a visual representation of the LSTM at time t. Note that at each time step, new information z_t is added to the model and both the factors and cell state are updated accordingly. Note also that, given the recurrent structure of the LSTM in which different lags are processed sequentially by the internal functions, the number of parameters is not a function of the lag structure. This essentially means that a larger number of lags does not imply in more parameters. If time steps far back in time are not relevant for the prediction, the algorithm updates the parameters accordingly.

The equations governing the internal flow of information of the LSTM can be written as

$$
\begin{aligned}
f_{t|L} &= \phi_{t|L} \odot tanh(c_{t|L}) \\
c_{t|L} &= \psi_{t|L} \odot c_{t-1|L} + \zeta_{t|L} \odot tanh(w_c' z_t + u_c' f_{t-1|L} + b_c) \\
\phi_{t|L} &= sigmoid(w_\phi' z_t + u_\phi' f_{t-1|L} + b_\phi) \\
\psi_{t|L} &= sigmoid(w_\psi' z_t + u_\psi' f_{t-1|L} + b_\psi) \\
\zeta_{t|L} &= sigmoid(w_\zeta' z_t + u_\zeta' f_{t-1|L} + b_\zeta) \\
f_{0|L} &= 0, \quad c_{0|L} = 0.
\end{aligned}
\tag{4}
$$

Intuitively, the cell state $c_{t|L}$ is updated recursively where a first filter $\psi_{t|L}$ controls what *past* information to retain, and a second filter $\zeta_{t|L}$ controls what *new* information to retain. The factors $f_{t|L}$ are themselves a function of the cell state where a final filter $\phi_{t|L}$ controls what information from the cell state to use for prediction.

In this application, I stack a fully connected FF to the LSTM structure to get the final prediction following common practice. Hence, the prediction of the model is given by $G(x_t; \Theta_h) = g_{FF}\Big(f_{t|L}\Big)$, with g_{FF} as defined in (3) and $f_{t|L}$ as in (4). A graphical representation of the full LSTM model is in Figure 3.

The parameters of the model are (i) those from the LSTM structure, $(w_{(j)}, u_{(j)}, b_{(j)})'$ for $j = c, \phi, \psi, \zeta$, where $w_{(j)} \in \mathbb{R}^{N \times p}$, $u_{(j)} \in \mathbb{R}^{p \times p}$, and $b_{(j)} \in \mathbb{R}^{p \times 1}$, as well as (ii) those from the FF network, $\{w_i, b_i\}_{i=1}^{q}$. The functions sigmoid and tanh are applied element-wise, and $\odot$ denotes the element-wise multiplication of two vectors. The hyperparameters are the number of LSTM factors p, the number of lags L, the number of nodes per layer n in the FF network as well as the number of layers q.

I consider estimating this model with two data sets: (i) the pool of economic predictors excluding inflation data, $x_t = (z_t, ..., z_{t-(L-1)})'$, referred as LSTM-pool, and (ii) the complete data set, $x_t = (z_t, ..., z_{t-(L-1)}, w_t, ..., w_{t-(L-1)})'$, referred as LSTM-all. The total number of parameters of the model amounts to $4(Np + p^2 + p) + (p+1)n + (Q-1)(n+1)n + (n+1)$.

2.3 The FF-LSTM model

The third model considered in this paper is constructed based on the two models described above. It can be viewed as an augmented FF-cpi model, where inflation data is combined to LSTM factors computed from the pool of macroeconomic predictors to form a composite input to a FF neural

Figure 3: The LSTM and FF-LSTM models

(a) The LSTM

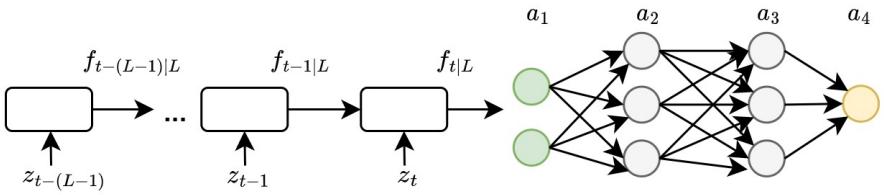

(b) The FF-LSTM

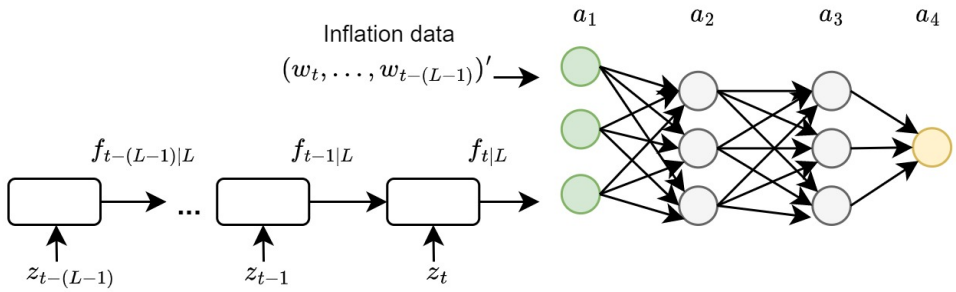

Schematic representation of the models. z_t is a vector collecting macroeconomic series except for price data, and w_t is a vector collecting price data. $f_{t|L}$ collects the LSTM factors at time t. The feed-forward network is represented with $q+1=4$ layers and $n=3$ nodes per hidden layer.

net. This model can be loosely associated with a factor-augmented distributed lag model, as it combines both types of inputs.

For clarification purposes, I rename the predictor sets as $x_t^w = (w_t, ..., w_{t-(L-1)})'$ and $x_t^z = (z_t, ..., z_{t-(L-1)})'$, and write $f_{t|L}(x_t^z)$ as the LSTM factors (here they are a function of the pool of macroeconomic predictors excluding price data). The FF-LSTM can then be defined as $G(x_t; \Theta_h) = g_{FF}\Big((x_t^w, f_{t|L}(x_t^z))'\Big)$, where g_{FF} is the FF network from (3), $f_{t|L}$ is as in (4), and Θ_h collects the parameters of $f_{t|L}$ as well as the FF network. Similarly to the LSTM model, the hyperparameters are the number of LSTM factors p, the number of lags L, the number of nodes per layer n in the FF network as well as the number of layers q. In this setting, the number of lags L is not restricted to be the same across predictor sets x_t^z and x_t^w. The number of parameters in this case amounts to $4(N^z p + p^2 + p) + (p + N^w L + 1)n + (Q-1)(n+1)n + (n+1)$, where I denote N^z and N^w to be the number of predictor series in x_t^z and x_t^w respectively. Figure 3 provides a graphical illustration.

3 On the selection of hyperparameters

A central part in the estimation of neural networks is the selection of hyperparameters, usually implemented via cross-validation. For a FF model, this could involve selecting the number of layers and the number of nodes per layer in the network, for instance. Given an optimal set of hyperparameters, out-of-sample performance is then computed using an additional sample previously unseen by the model. In this paper, I use a modified version of the traditional *k-fold* cross-validation that accounts for the autocorrelation inherent of time series. A more detailed description of the cross-validation procedure is available in Appendix D.

Table S2 indicates the hyperparameters considered for cross-validation in this application, as well as the candidate and optimal values. For instance, the number of lags L of predictors to be included in the model is a hyperparameter for which I select within the set $\{6, 12, 24, 48\}$. The data used to estimate and cross-validate the models ranges from March-1959 to July-2006 (see Figure S1). As I also report results on the out-of-sample period starting from May-1993, I repeat the cross-validation process using only data prior to May-1993 as well. However, the resulting optimal hyperparameters using this later sample are found to be very similar to the ones reported in Table S2. For the cases where the hyperparameters are not the same, results on forecast performance are not qualitatively different. For this reason, I opt to set the same hyperparameters as in Table S2 for both out-of-sample periods considered in the analysis.

A closer examination of the selected hyperparameters reveals that the networks are quite large. For example, the number of nodes is selected to be the upper bound of the grid-search values $\{16, 32, 64, 128\}$ for all models, that is $n = 128$. This means that the networks have huge amounts of parameters, i.e. $700K+$ for the FF-pool, or even $50K+$ for the LSTM models. Despite the common empirical knowledge that these models are able to handle cases with a much larger number of parameters than observations, practitioners may be interested in comparing the performance of such big models (i.e. networks with a disproportionately large amount of parameters than observations) to smaller networks in which we fix *ex-ante* specific hyperparameters without the need to cross-validate those. Obvious advantages of considering fixed, small networks are a simplified cross-validation step and smaller computational burden. In order to provide insights on these issues, I consider estimating an additional set of models that share the same selected hyperparameters as before, except for the number of nodes n, which is fixed to be 4 for all models (I set 4 as an arbitrary small number). The number of nodes n has by far the highest weight in

the total number of parameters, which is decreased by approximately 98% across models when fixing $n = 4$ (e.g. from 51,017 to 1,125 in the case of the LSTM-pool, and from 758,273 to 22,725 for the FF-pool; see Table S3). Additionally, fixing only one hyperparameter, instead of multiple, facilitates the comparison. For instance, if one would also fix the number of lags to be smaller, it would be unclear whether differences in forecast performance are due to model complexity or the lag structure. Section 6 discusses the differences in out-of-sample performance between the networks specified by the cross-validation step and the smaller networks as just defined.

4 Data

The data used in the empirical study is collected from the FRED-MD data base, a compilation of monthly US data made available by McCracken and Ng (2016), and corresponds to the vintage of October 2019. This data set comprises 128 series with 730 observations each, spanning the period from January-1959 to October-2019. Table S1 in Appendix A provides the description of all the series in the data set as well as information on the data transformation.

The series undergo a sequence of transformations before estimation. First, I transform the data following McCracken and Ng (2016) to guarantee stationarity (column Tcode in Table S1). The only exceptions are aggregate CPI and aggregate PCE (items No. 110 and 120 respectively in Table S1), which are transformed in log differences. The inflation target in the paper is then defined as $\pi_t = log(P_t) - log(P_{t-1})$, where P_t is either aggregate CPI or aggregate PCE at time t. Second, missing observations are replaced using the iterative expectation-maximization (EM) algorithm from Stock and Watson (2002) (the percentage of missing values for each series is reported in Table S1). Finally, for the estimation of the neural network models, the data is further normalized within the interval $[-1, 1]$. The normalization is carried out in-sample and extrapolated to the out-of-sample period to avoid look-ahead bias. This transformation is appropriate here since the evidence suggests that neural nets perform better when the regressors share a similar order of magnitude.[3] This scaling is similar to assuming an equal importance of covariates *ex-ante*.

After data transformations, I collect into w_t the price series corresponding to items No. 110 to 119 when targeting CPI, or items No. 120 to 123 when targeting PCE, from Table S1. In contrast, z_t corresponds to all macroeconomic series from Table S1 that are not in w_t. For instance, when targeting CPI, z_t includes all series except items No. 110 to 119.

[3]This fact is related to the gradient descent optimization process, which seems to converge much faster when the regressors are normalized (Ioffe and Szegedy, 2015). For details on the optimization procedure, see appendix C.

5 The LSTM factors

The LSTM and FF-LSTM models work as a dimensionality-reduction tool, as they squeeze the input information from a potentially large set of variables into a p-dimensional vector $f_{t|L}$, collecting what is referred as LSTM factors. In this section, I compare these factors with those extracted from PCA as well as business cycle indicators. I show that the estimated factors, in addition to reducing the dimensionality, also convey information on variable selection relevant for prediction, as per the supervised nature of the estimation, as discussed previously.

I extract LSTM factors by evaluating the estimated models over the full sample period, and obtain $f_{t|L}$ for $t = L + h, ..., T$.[4] However, as the estimation of neural networks can be sensitive to initial values, these models are generally estimated as an ensemble over neural networks embedding different initializations (see Section 6.1 for more details). In order to recover a unique set of LSTM factors, I therefore estimate K models $\{\mathcal{M}_k\}_{k=1}^K$ with different initial values, and select the model $\mathcal{M}_k$ with lowest out-of-sample error over a validation set. This essentially implies selecting an optimal initialization.

To shed light on the information encoded into the LSTM factors, Table 1 shows how these factors relate to each group of variables from the set of predictors $\mathcal{Z}$, and offers a comparison with standard PCA factors. The entries correspond to the squared correlation between the factors and each variable in $\mathcal{Z}$, averaged across groups. Three points stand out. First, LSTM factors are generally loaded on common predictors of inflation, e.g. prices, interest & exchange rates, housing starts, employment. Second, apart from the anticipated high correlation with CPI and PCE variables, LSTM factors are significantly loaded on housing starts. This group was previously reported in the literature as important for predicting inflation (see for instance Stock and Watson, 1999 and Bai and Ng, 2008). Third, FF-LSTM factors tend to be *more* correlated with real variables (housing, output and labour market) and *less* correlated with price variables than the LSTM-pool or LSTM-all factors, especially at large horizons. Recall that the factors extracted from the LSTM-pool and the FF-LSTM both receive the pool of macroeconomic predictors excluding price data as inputs, but that the FF-LSTM observes price information separately that it uses to improve the forecast. The fact that FF-LSTM factors give relatively less weight to price information and relatively more weight to real variables suggests that these factors work as filters: They filter out from the pool of macro predictors the signals to forecast inflation that are less related to prices,

[4]The number of factors as well as other hyperparameters are selected via cross-validation according to Table S2.

Table 1: Variance decomposition of LSTM factors

			Out&Inc	Lab Mkt	Hous	Orders	Mon&Cr	Stock Mkt	IR&ER	Prices	CPI/PCE
Principal components											
PC1			0.35	0.26	0.31	0.16	0.02	0.07	0.06	0.00	0.02
PC2			0.03	0.02	0.13	0.09	0.01	0.06	0.19	0.03	0.47
Neural network models											
LSTM-pool	3	f1	0.01	0.04	0.15	0.06	0.01	0.01	0.07	0.01	0.21
		f2	0.01	0.01	0.01	0.07	0.01	0.01	0.16	0.01	0.33
	6	f1	0.05	0.05	0.16	0.02	0.01	0.02	0.04	0.00	0.21
		f2	0.01	0.03	0.28	0.04	0.01	0.00	0.07	0.00	0.25
	12	f1	0.00	0.01	0.01	0.04	0.01	0.00	0.05	0.01	0.20
		f2	0.02	0.04	0.11	0.09	0.01	0.02	0.11	0.01	0.27
	24	f1	0.00	0.02	0.20	0.03	0.01	0.00	0.07	0.00	0.13
		f2	0.00	0.04	0.04	0.03	0.01	0.01	0.08	0.00	0.31
LSTM-all	3	f1	0.00	0.02	0.09	0.05	0.01	0.00	0.07	0.01	0.38
		f2	0.03	0.05	0.03	0.09	0.01	0.01	0.10	0.01	0.24
	6	f1	0.01	0.02	0.05	0.07	0.01	0.04	0.19	0.01	0.45
		f2	0.00	0.03	0.03	0.03	0.01	0.01	0.05	0.00	0.20
	12	f1	0.02	0.04	0.35	0.03	0.01	0.00	0.01	0.00	0.06
		f2	0.05	0.11	0.08	0.06	0.01	0.02	0.05	0.01	0.00
	24	f1	0.08	0.07	0.39	0.02	0.01	0.01	0.02	0.01	0.01
		f2	0.00	0.02	0.08	0.06	0.01	0.02	0.10	0.02	0.32
FF-LSTM	3	f1	0.01	0.02	0.11	0.09	0.01	0.02	0.11	0.00	0.30
		f2	0.04	0.09	0.19	0.09	0.01	0.00	0.06	0.00	0.20
	6	f1	0.02	0.02	0.05	0.06	0.01	0.08	0.16	0.01	0.34
		f2	0.09	0.10	0.47	0.07	0.01	0.01	0.04	0.00	0.09
	12	f1	0.04	0.06	0.39	0.07	0.01	0.00	0.03	0.00	0.10
		f2	0.04	0.08	0.19	0.10	0.01	0.01	0.11	0.00	0.09
	24	f1	0.13	0.16	0.18	0.04	0.01	0.05	0.04	0.00	0.01
		f2	0.04	0.05	0.45	0.03	0.01	0.00	0.02	0.00	0.01

This table presents the average variance decomposition of the estimated LSTM factors (and the first two PCA factors) across groups of variables (groups as defined in McCracken and Ng, 2016). The entries correspond to the squared correlation between the factors and each variable in the original data set $\mathcal{Z}$, averaged across groups. 'Prices' excludes CPI and PCE, which are shown in the last column separately. Results are reported for the $p = 2$ LSTM factors at horizons $h = 3, 6, 12, 24$. Darker shades of grey correspond to higher values.

Figure 4: Individual variable importance in LSTM factors

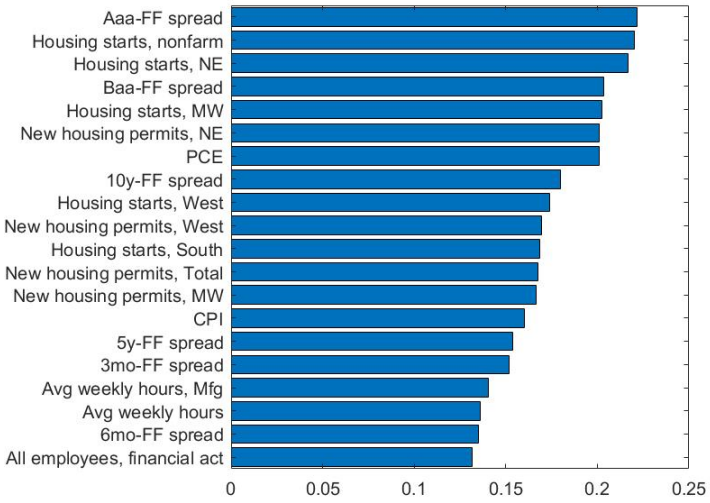

The entries correspond to the squared correlation between LSTM factors and each variable in $\mathcal{Z}$, averaged across models (LSTM-pool, LSTM-all, FF-LSTM), fators (f1 and f2), and horizons (3, 6, 12, 24). Presented are the 20 variables with higher loadings.

since the later is already being provided to the model separately. I borrow from these insights and interpret FF-LSTM factors as "output-driven" and LSTM-pool/LSTM-all factors as "price-driven" in the visual comparison with macroeconomic indicators below.

To dig deeper into variable importance embedded into the LSTM factors, Figure 4 shows the 20 variables in $\mathcal{Z}$ presenting the higher loadings. The entries are the same as in Table 1, i.e. the squared correlation between the factors and the variables, only this time they are averaged across models (LSTM-pool, LSTM-all, FF-LSTM), factors (f1 and f2), and horizons (3, 6, 12, 24). High-yield corporate bond spreads stand out, together with housing starts and permits. PCE and CPI can be categorized as the third most important group, followed by labor market variables, with 20+ variables appearing right below in the ranking (not reported).

Looking at the dynamics, Figure 5 plots selected factors over time for horizons $h = 12, 24$. In subplot (a), note how price-driven factors are correlated with headline inflation (0.73 at $h = 12$, and 0.56 at $h = 24$). Compared to PC2, the principal component more correlated with prices (see Table 1), LSTM factors seem to better capture the downward trend of inflation in the second part of the sample, and are less volatile. The plot also shows the long-term trend of CPI inflation according to the Survey of Professional Forecasters (SPF) for comparison. This may indicate that the LSTM can be useful at detecting low frequency components.

Figure 5: The LSTM factors

(a) Price-driven factors

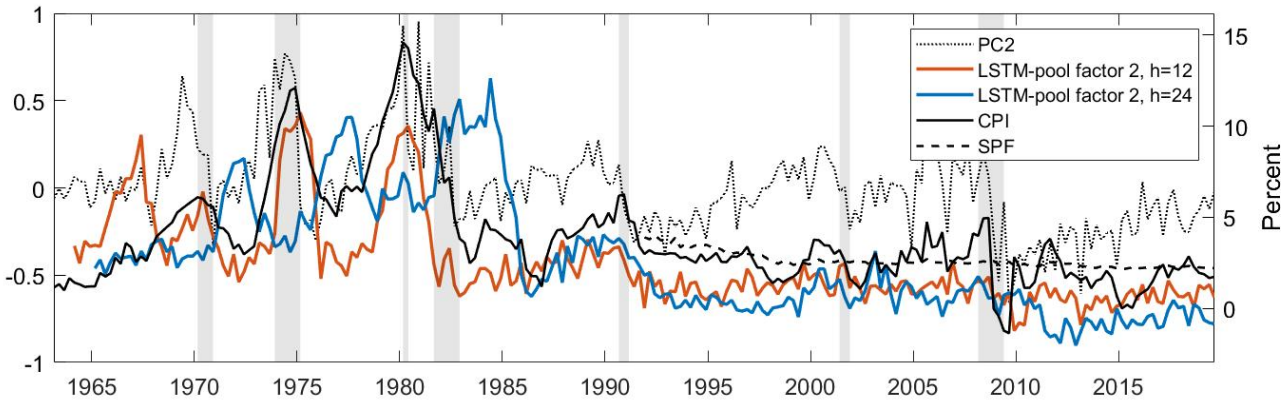

(b) Output-driven factors

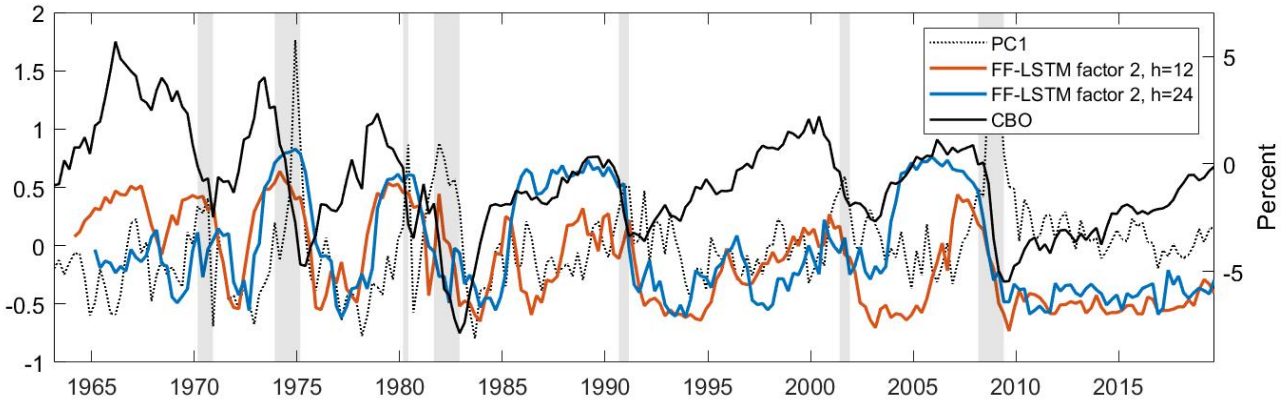

The figure plots selected LSTM factors estimated from the LSTM-pool (subplot (a)) and FF-LSTM (subplot (b)) over the full sample period $t = L + h, ..., T$, at horizons 12 and 24. The forecasting target is CPI inflation. For comparison, the plots also show the first two principal components (PC1 and PC2) estimated form the input data $\mathcal{Z}$, as well as headline CPI inflation, 10-year CPI inflation according to the Survey of Professional Forecasters (SPF), and the output gap from the Congressional Budget Office (CBO). The grey areas are NBER recessions. The LSTM factors and principal components are plot on the left axis (series are normalized), and the other series on the right axis (percent).

Subplot (b) shows factors from the FF-LSTM model and highlights its similarity with the business cycle. I compare the LSTM factors with the output gap produced by the Congressional Budget Office (CBO), NBER recessions and PC1. Interestingly, note how the factors lag the CBO's output gap measure while being relatively correlated with the later (0.53 at $h = 12$, and 0.45 at $h = 24$). This again speaks to the ability of the LSTM to condense macroeconomic data in an economic-meaningful way, as the model seems to successfully detect business cycle fluctuations. Additionally, given that LSTM factors are estimated within a prediction context, these findings are

consistent with Phillips curve-based models, since output gap-type signals appear as an important inflation predictor themselves (other recent works emphasizing a revival of Phillips curve methods are e.g. Hasenzagl et al., 2022 and Coulombe, 2022). It is interesting to note that during the post-Global Financial Crisis (GFC) period, the FF-LSTM factors remain at its lowest historic levels and are more pessimistic than the CBO's measure of the output gap. This may be an indication that the *de facto* recovery may have been more sluggish than previously thought.

It is worth mentioning that the small number of LSTM factors used above is a direct consequence of the cross-validation design, in which the number of factors is restricted to be within the set $\{2, 4, 6, 8\}$ (see Table S2 on hyperparameter selection). This is a modelling choice that facilitates interpretation and comparison with PCA and other factor structures usually encountered in the empirical literature. For instance, McCracken and Ng (2016) report the optimal number of factors estimated from the FRED-MD database to be between 2 and 8 in the context of a standard factor model, using a similar sample period than the present analysis. For the practitioner mainly concerned with forecast performance, it may be advisable to investigate a finer grid of number of factors.

6 Forecast performance

This section compares the forecast performance of neural networks with common benchmarks from the literature of inflation forecasting and alternative machine learning models. These comprise the autoregressive model of order p, or $AR(p)$, the factor model (Fact), the unobserved components with stochastic volatility model (UCSV), the random forest (RF), as well as shrinkage methods, LASSO, Ridge regression and the Elastic-net (ENet). The description of the benchmarks is in Appendix G.

Forecasts are computed in a rolling window basis. At each time step, a window of R observations is used to estimate the models (and to cross-validate hyperparameters), and forecast performance is averaged over P out-of-sample (OOS) observations. The total number of observations in the sample is equal to $T = R + P + h - 1$, where h is the forecast horizon. Note that R changes with the forecast horizon, as T and P are fixed. Following standard practice, I evaluate

forecast performance using the Root Mean Squered Error (RMSE),

$$RMSE_{h,m} = \sqrt{\frac{1}{P}\sum_{t \in OOS}(\pi_t - \hat{\pi}_{t,m})^2},$$

where $\hat{\pi}_{t,m}$ is the prediction of model m at time t. To compare models, I employ a standard Diebold and Mariano (1995) (DM) test with respect to the $AR(p)$, as well as the Model Confidence Set (MCS) proposed in Hansen et al. (2011). Given an initial set of predictive models, the MCS is the subset (potentially equal to the original) that contains the best model at a given level of confidence. I use 5000 bootstrap samples to construct the MCS test statistics, and compute 75% model confidence sets following the original paper.

For the neural networks, I re-estimate the models at every 4 years during the OOS period.[5] Results are presented for two distinct OOS periods, (i) May-1993 to July-2006, and (ii) August-2006 to October-2019, the second period covering the GFC and featuring more volatile inflation. Results refer to models with CPI inflation as the main target (similar analysis is done for PCE inflation in Appendix E).

6.1 Predictions as an ensemble

The usual non-convex loss function of neural networks implies that the estimated parameters are in general very sensitive to initial values.[6] In practice, this means that the neural network predictions will be very much dependent on the initialization. To overcome this issue, the empirical literature usually adopts the solution of averaging out the predictions from models estimated with different initial values (see e.g. Izmailov et al., 2019, Fort et al., 2020, and Wilson and Izmailov, 2022 for papers exploring model averaging in the context of deep neural nets).

Consider the set of models $\{\mathcal{M}_k\}_{k=1}^K$ estimated from the same neural network architecture but with different initial values. Let $\{\hat{y}_{k,t+h}\}_{t=1}^P$ be the forecast associated with model $\mathcal{M}_k$, where P is the OOS size. The ensemble prediction at period $t+h$ is defined as $\hat{y}_{ens,t+h} = \frac{1}{K}\sum_{k=1}^K \hat{y}_{k,t+h}$, which is essentially a model-averaging technique that attributes an equal weight to each forecast $\hat{y}_{k,t+h}$. Section 7 shows empirically that this solution is at least as good as the individual forecasts in terms of mean squared error according to a standard DM test procedure.

[5] I opted for this solution to improve computational time, although a more frequent re-estimation of the neural network models, e.g. every year, may improve performance.

[6] Initial parameters are randomly drawn from a specific uniform distribution (Appendix C).

I therefore adopt this ensemble technique and estimate each neural network $K = 1400$ times letting vary the initialization.[7] The main OOS results reported below refer to the ensemble prediction $\hat{y}_{ens,t+h}$ across the 1400 forecasts.

6.2 Out-of-sample results

Table 2 presents the OOS results. The entries are loss ratios with respect to the $AR(p)$ model. A glance at Table 2 reveals that neural networks performance is competitive against benchmarks, although not outstanding. Specifically, neural nets can present substantial forecasting gains (e.g. RMSE ratios ≈ 0.85), but these are not robust across models and horizons. LSTM-only models (LSTM-pool, LSTM-all) in particular tend to present a satisfactory forecast performance at long horizons as well as at horizon 1. On the other hand, the performance of FF models (FF-cpi, FF-pool, FF-LSTM) changes with the sample and the input data. I analyse below the local forecasting performance, as opposed to the average performance, to shed more light on these points. It is interesting to note that adding information on the state of the economy usually helps in forecast performance (FF-LSTM model as opposed to the FF-cpi model). Conversely, adding price information when the pool of macro predictors is already taken into account does not seem to improve the prediction significantly (LSTM-all as opposed to LSTM-pool). It is worth mentioning that the random forest stands out overall across the different scenarios and forecast horizons, a finding that is in line with previous literature (Medeiros et al., 2019). Also note that the performance of the neural nets and some benchmarks improves in the 2006-2019 period with respect to 1993-2006 (especially when predicting PCE inflation; see Table S4). This fact resonates the common understanding that machine learning models tend to outperform traditional benchmarks during the post-GFC period of heightened macroeconomic uncertainty and more volatile inflation (see for instance Medeiros et al., 2019 and Buckmann and Joseph, 2022 for applications to inflation and unemployment respectively).

On the comparison between large and small networks, the former specified by cross-validation and the later by networks with 4 nodes per layer, I discuss a few takeaways. First, the performance of small networks is in general worst (in the sense of DM tests) than large ones, but there are exceptions. Specifically, smaller networks appear to help the performance of LSTM models at medium horizons (6 in particular) for the 2006-2019 sample (note that this gain in accuracy comes

[7] In order to guarantee optimal computational time, the number of iterations was chosen such that it is proportional to the number of available processors.

Table 2: Out-of sample forecast performance for CPI inflation

	1993-2006					2006-2019				
	1	3	6	12	24	1	3	6	12	24
Benchmark models										
UCSV	1.02	**1.07**	1.00	1.07	**0.91****	**1.08**	0.99	**0.98**	**1.02**	**1.02**
Fact	1.00	**1.00**	1.01	1.04	**0.99**	**0.95**	**1.00**	**1.01**	**1.03**	**1.02**
RF	**0.88*****	**0.98**	**0.96***	**0.92*****	**0.92***	**0.99**	**0.89*****	**0.90*****	**0.94*****	**0.94*****
LASSO	**0.91*****	**0.96**	**0.97****	1.01	**1.01**	**0.95*****	**0.94****	**0.95*****	**0.94*****	**0.91*****
Ridge	0.94**	1.01	1.02	**0.98**	**0.93*****	**1.03**	1.15	**1.35**	1.23	1.36
ENet	**0.91*****	**0.96***	**0.97****	1.01	**1.01**	**0.93*****	**0.93*****	**0.95*****	**0.93*****	**0.90*****
Neural network models										
Large architecture										
FF-cpi	**0.85*****	**0.92****	**0.91*****	**0.98**	**1.07**	**1.04**	**0.97**	**0.98**	**1.01**	**0.94*****
FF-pool	0.99	**0.97**	**0.96***	**0.93*****	**0.94***	**1.05**	**0.85*****	**0.87*****	**0.95**	**0.99**
LSTM-pool	**0.85*****	1.08	1.08	**0.93****	**0.98**	**0.94***	**0.88****	**1.02**	**0.95***	**0.93*****
LSTM-all	**0.84*****	1.08	1.08	**0.93***	**0.97**	**0.93****	**0.88****	**1.03**	**0.95**	**0.94****
FF-LSTM	**0.85*****	**0.92***	**0.92*****	**0.97***	**1.05**	**1.02**	**0.94***	**0.96**	**0.98**	**0.92*****
Small architecture										
FF-cpi	**0.91***	**0.96**	**0.96**	1.02	1.06	1.07	**0.97**	**0.97**	**1.01**	**0.99**
FF-pool	1.00	1.04	1.01	**0.95****	**0.91*****	**1.06**	**0.88****	**0.90****	**0.98**	**1.02**
LSTM-pool	**0.89****	1.12	1.11	**0.95***	**0.97**	**1.00**	**0.87*****	**0.89****	**0.94*****	**0.96****
LSTM-all	**0.89****	1.11	1.11	**0.95***	**0.94***	**0.99**	**0.88*****	**0.89****	**0.94****	**0.96****
FF-LSTM	**0.88****	**0.98**	**0.96**	**0.96***	**0.95***	**1.01**	**0.91****	**0.92****	**0.97**	**0.95****

The table presents the loss ratios with respect to the $AR(p)$ model for horizons $h = 1, 3, 6, 12, 24$ and two OOS periods. The target is CPI inflation. *Large architecture* and *Small architecture* refer to models specified as in table S2 and S3 respectively. The loss function is the RMSE. *, **, *** denote significance of the one-sided DM test at a 10%, 5% and 1% levels respectively. Models retained in the 75% MCS are in bold.

entirely from the FF network stacked to the LSTM). Second, forecasting gains of smaller networks remain substantial. This suggests that overly complex networks do not necessarily guarantee a better performance. These same insights follow for PCE (Table S4). In general, these results speak in favor of ensemble techniques that take into account not a single architecture but multiple if the interest remains solely in forecast performance. Regarding computational time, despite the large difference in the number of parameters in this application, small networks were on average only 30% faster than larger ones, which doesn't seem to compromise the use of the latter within cross-validation or ensemble model designs.

In order to get a clearer picture of the models' performance over time, I employ the Fluctuation Test introduced in Giacomini and Rossi (2010). The proposed statistic tests for an equal forecast

accuracy of two different forecast series and is robust to instability on their relative forecast performance. The statistic is much similar to the DM test procedure, except that it is computed over a rolling window of fixed size $m = 48$. In this application, I use the one-sided test where the rejection of the null hypothesis (i.e. a test statistic larger than the critical value) implies that the candidate forecast series of each neural net is statistically superior to the $AR(p)$ benchmark for a given observation in the OOS period. The value of m is chosen such that $m/P \approx 0.3$, in which case the one-sided critical value at the 5% confidence level is 2.77 according to Giacomini and Rossi (2010). Figure 6 shows the implied test statistics over time at selected horizons with the CPI as main target, and focuses on the case of large architectures, i.e. models selected via cross-validation. (In the plots, I do not include the LSTM-all and FF-LSTM models as their overall performances are very similar to the LSTM-pool and FF-cpi models respectively, and I henceforth refer to the LSTM-pool as simply LSTM in this section).

I discuss three points. First, the LSTM model seems suitable to forecast during periods of higher macroeconomic uncertainty as was the case in the post-GFC period (2006-2019). Note how the LSTM is superior to the $AR(p)$ (as well as the FF models to some extent) for horizons 1 and 24 (Figure 6) and horizons 3 and 6 (Figure S2 in the appendix). The prediction plots reveal that this is mainly because the LSTM is on average less affected by sudden, short-lived movements in prices compared to other models. For instance, some models are very sensitive to the downward pressure on prices caused by the GFC, as is the case of the $AR(p)$, but also the random forest (plot not reported).

Second, the LSTM appears to be a good model at long horizons, a finding that is robust to the OOS period and network architecture, while forecasting gains can be found at very short horizons as well, depending on the sample. Results for medium horizons are somewhat mixed, as it generally depends on the architecture. More specifically, the prediction plots at horizon 1 show that the LSTM adapts quite well to short term movements in inflation, e.g. note in particular the second half of the 1993-2006 sample. However this is not a particularity of the LSTM, as the FF-cpi and FF-LSTM models are as good. At the longest horizon, the LSTM maintains a good forecast accuracy during the majority of the sample in both OOS periods. The long-term predictions of the LSTM tend to be quite smooth and to match the direction of inflation 24 steps ahead, suggesting an ability to predict well the trend of the series. There is one exception to the good performance of the LSTM at horizon 24 in the end of the 1993-2006 sample, which drives the modest average result reported in Table 2. The prediction plot helps understand that episode,

Figure 6: Local forecast accuracy and Predictions for CPI inflation

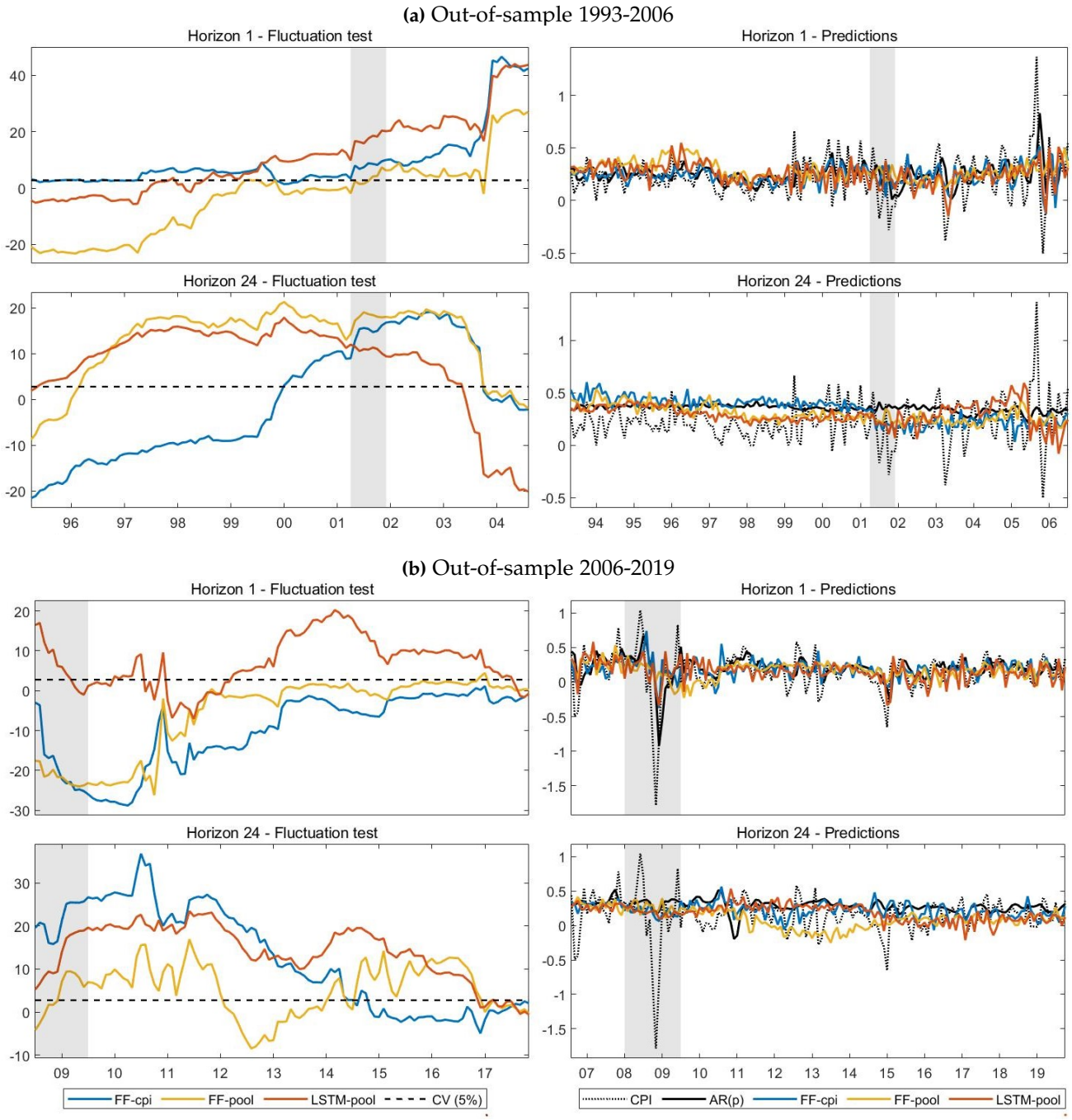

First column: Test statistics according to the Fluctuation Test from Giacomini and Rossi (2010); values above the dashed line indicate that the underlying model presents better forecast accuracy than the $AR(p)$ benchmark over a window of fixed size at the 5% confidence level. Second column: Predictions of selected models; the scale is $100\times$ log differences. Gray areas are NBER recessions.

which is characterized by a large swing in headline inflation. The LSTM did particularly bad and the $AR(p)$ particularly well, where the latter predicts a stable trend. Looking at medium horizons, LSTM models do not appear to be good predictors in general, although the small networks show gains at the 2006-2019 sample, suggesting that the poor performance can be in fact related to the stacked FF architecture. It seems that at these horizons the LSTM predictions are somehow more "erratic" than those of FF and autoregressive models (Figure S2), which on average contributes negatively to its performance. In fact, the good average performance of the LSTM reported at horizon 3 is purely driven by the GFC episode, where the $AR(p)$ is particularly bad.

Finally, results from the FF models are mixed. For instance, during the 1993-2006 OOS period, the FF-cpi (and the autoregressive model) cannot track well the downward trend in inflation in the middle part of the sample at horizon 24, while the FF-pool is more successful. On the other hand, during 2006-2019, it is the FF-pool that shows the worst performance at horizon 24, where it underestimates inflation over a significant part of the sample.

Overall, the recursive structure inherent to the LSTM, when compared to FF networks, appears to grant more robustness to predict at long horizons, but can hurt its performance at the medium term. Results on FF models are less conclusive, although their performance remains competitive against benchmarks. An important takeaway in terms of forecast performance is the sensitivity with respect to network architecture, and the practitioner solely interested in forecast performance would be advised to consider ensemble techniques that decrease the variance of single picked architectures, even if those are selected over a validation sample.

7 Uncertainty over network initialization

Neural network predictions can in general be sensitive to the the choice of initialization as well as network architecture as discussed above. In fact, machine learning models more generally are prone to instabilities in performance due to their sensitivity to model specification. D'Amour et al. (2022) refers to this issue as underspecification and caution on the transferability of these models from the lab to real-world applications (see also Geirhos et al., 2020 and Buckmann and Joseph, 2022 for similar discussions).

In this section, I contribute to this debate by focusing on the dependence of network predictions on initial values. As discussed previously, ensembles are usually appropriate in this case to smooth out predictions. Natural questions that emerge are how different are the performances of forecasts

embedding different initializations, and more importantly how the performance of the ensemble forecast $\{\hat{y}_{ens,t+h}\}_{t=1}^{P}$ compares with the performance of individual forecasts $\{\hat{y}_{k,t+h}\}_{t=1}^{P}$, for $k = 1, ..., K$. To address these points, I compute a standard DM test statistic of equal forecast accuracy between the individual forecasts $k = 1, ..., K$ and the ensemble forecast. This exercise essentially yields a distribution of the DM test statistic over specifications embedding different initial values.

Let $\{e_{k,t+h}\}_{t=1}^{P}$ and $\{e_{ens,t+h}\}_{t=1}^{P}$ be forecast errors associated with forecast $\{\hat{y}_{k,t+h}\}_{t=1}^{P}$ and with the ensemble forecast $\{\hat{y}_{ens,t+h}\}_{t=1}^{P}$ respectively over the OOS period. Now consider a loss-differential series $\{d_{k,t+h}\}_{t=1}^{P}$, where $d_{k,t+h} \equiv [e_{k,t+h}^2 - e_{ens,t+h}^2]$, such that positive values are associated with a better performance of the ensemble prediction. For a given horizon h, I compute

$$\Delta_{k,h} = \frac{\bar{d}_{k,h}}{\hat{\sigma}_d / \sqrt{P}}, \qquad k = 1, ..., K, \tag{5}$$

where $\bar{d}_{k,h} = \frac{1}{P} \sum_{t=1}^{P} d_{k,t+h}$ is the sample mean loss-differential, and $\hat{\sigma_d}^2$ is a heteroskedasticity and autocorrelation consistent (HAC) estimate of the variance of $\bar{d}_{k,h}$.

I discuss two potential issues with the use of the DM statistic on nestedness and parameter estimation error. For the former, the statistic seems appropriate as the two series being compared here can be better described as coming from different forecast strategies rather than models (see discussion in Diebold, 2015). Indeed, on the one hand we have a forecast from a neural net with initialization k and on the other a forecast equal to the mean of K different neural net forecasts, each with a different initialization. However, to alleviate the concern of nestedness regarding the use of the DM statistic, I also consider the mean squared error-adjusted test from Clark and West (2007), which is equivalent to an encompassing test and suitable in the context of nested models. This extended result is shown in Appendix F and briefly discussed below. On parameter estimation error, I note that the implied assumption from Diebold and Mariano (1995) that the ratio P/R vanishes asymptotically is violated, as here $P/R \approx 0.50$ or larger. However, as pointed out in Corradi and Swanson (2006), if the same loss function is used for both estimation and model selection purposes, which is the case in the paper (mean squared error loss), the contribution of parameter estimation error in the DM statistic becomes negligible.

I carry out the analysis considering the neural net models estimated in the previous section (as defined in Table S2), for $h = 1$ and $h = 24$, and $K = 1400$ different initializations as before. Figure 7 plots the distribution of the statistic $\Delta_{k,h}$ over $k = 1, ..., K$ for each model. Also plotted are the

Figure 7: Distribution of the DM statistic over different initializations

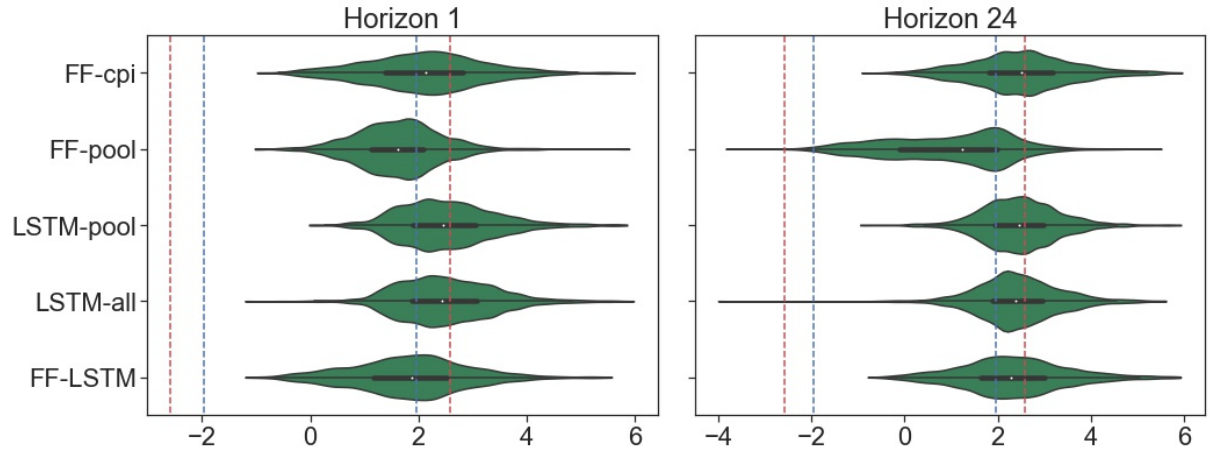

DM test statistic $\Delta_{k,h}$, for $k = 1, ..., 1400$ and horizons $h = 1, 24$. Positive values imply better forecast performance of the ensemble prediction over predictions from a particular initialization. Vertical dashed lines are Gaussian critical values at the 5% (blue) and 1% (red) significance levels. Values are truncated at 6 for visualization purposes.

Gaussian critical values at the 5% (blue dashed line) and 1% (red dashed line) significance levels.

The plots show that, in most cases, the means of the DM distributions lie beyond the 5% line, indicating that the ensemble is on average better than any single initialization at the 5% level of significance. In fact, on average across models and horizons, around 60% of different initializations are statistically worse than the ensemble at the 5% level, while the remaining 40% (except for a few outliers) are not significantly different from the ensemble prediction. Additionally, there are no large differences across models. The same conclusions follow if one looks at the mean squared error-adjusted test, instead of the DM test, shown in Figure S3 in the appendix. As expected, in this later case we observe higher values of the statistics, as the test corrects for the potential upward bias of the alternative model (here, the ensemble) under the null that its additional parameters are zero.

This exercise also reveals that predictions from models with different initial values can be substantially different (note the large variation of the test statistic across k's).[8] Individual predictions of the FF-pool, in particular, exhibit substantial variation (Figure S4 shows that the same is true for other horizons). Figure S5 (in Appendix F) disentangles the contributions of the loss-differential mean and standard deviation within the DM statistic. Note that predictions from the FF-pool can be much more sensitive to the choice of initialization compared to the

[8] Buckmann and Joseph (2022) have similar findings, where the authors show that neural networks and support vector machines can be particularly sensitive to initial conditions compared to other machine learning models.

FF-cpi. Both the mean and standard deviation of the loss-differential can take on relatively high values, which explains the higher dispersion in DM statistics of the FF-pool compared to other models. Interestingly, the salient difference between the FF-pool and the FF-cpi is the number of parameters (Table S2), suggesting that larger networks, all else equal, can create additional instabilities in model predictions.

Overall, this evidence substantiates the use of neural network ensembles given the sensitivity to initial values and network architecture (Section 6.2 also discusses the dependence of forecast performance on architecture). Additionally, due to the highly nonlinear setting, it is plausible that the best initial values change over time. Combining the outcome of different forecasts in an ensemble-like approach is therefore a way of making the final prediction more robust to this type of uncertainty.

8 Concluding remarks

This paper investigates the suitability of a recurrent neural network, specifically the LSTM, to forecast inflation, while analysing advantages and drawbacks of using this model in terms of interpretability and implementation. On forecast performance, LSTM-based models are good at forecasting the long-term trend of the inflation series and perform well during periods of higher macroeconomic uncertainty, such as during the post-GFC period. This is due to their lower sensitivity to temporary and sudden price changes compared to traditional models in the literature. However, their overall forecasting performance is not outstanding, especially compared to the random forest model. The analysis also reveals that factors generated by the estimation of LSTM models capture the long-term trend of inflation, along with output gap-type signals, which is consistent with a Phillips curve-based specification. Finally, the paper sheds light on the sensitivity of neural network's predictions to initial values and network size. Specifically, networks of different sizes generally result in different predictions, and larger networks do not necessarily outperform smaller ones. Additionally, neural networks' predictions are significantly sensitive to the initialization, where large enough networks can exacerbate this sensitivity even more. Practitioners interested in forecasting performance should, therefore, consider the use of ensemble techniques to average out the variation from both initial values and network size (or network architecture in general), which significantly stabilizes predictions.

References

Almosova, A., and N. Andresen. (2019). "Nonlinear inflation forecasting with recurrent neural networks." .

Andreini, P., C. Izzo, and G. Ricco. (2020). "Deep dynamic factor models." arXiv:2007.11887 .

Athey, S. (2019). "The Impact of Machine Learning on Economics." In "Ajay Agrawal, Joshua Gans, and Avi Goldfarb (Eds.), The Economics of Artificial Intelligence: An Agenda," 507–547, Chicago: University of Chicago Press.

Atkeson, A., and L. E. Ohanian. (2001). "Are Phillips curves useful for forecasting inflation?" Quarterly Review, Federal Reserve Bank of Minneapolis 2–11.

Bai, J., and S. Ng. (2008). "Forecasting economic time series using targeted predictors." Journal of Econometrics 146, 2, 304–317.

Breiman, L.. (2001). "Random Forests." Machine Learning 45, 5–32.

Breiman, L., J. H. Friedman, R. A. Olshen, and C. G. Stone (1984). Classification and regression trees. Wadsworth International Group, Belmont, California, USA.

Buckmann, M., and A. Joseph. (2022). "An interpretable machine learning workflow with an application to economic forecasting." Bank of England Working Paper No 984 .

Chakraborty, C., and A. Joseph. (2017). "Machine learning at central banks." Bank of England Working Papers 674.

Choudhary, M. S., and A. Haider. (2012). "Neural network models for inflation forecasting: an appraisal." Applied Economics 44, 20, 2631–2635.

Clark, T. E., and K. D. West. (2007). "Approximately normal tests for equal predictive accuracy in nested models." Journal of Econometrics 138, 291–311.

Cook, T. R., and S. Hall. (2017). "Macroeconomic Indicator Forecasting with Deep Neural Networks." In "Federal Reserve Bank of Kansas City, Research Working Paper 17-11," .

Corradi, V., and N. R. Swanson. (2006). "Chapter 5 Predictive Density Evaluation." volume 1 of Handbook of Economic Forecasting, 197–284, Elsevier.

Coulombe, P. G.. (2022). "A neural Phillips curve and a deep output gap." Available at SSRN: https://ssrn.com/abstract=4018079 .

Coulombe, P. G., M. Leroux, D. Stevanovic, and S. Surprenant. (2020). "How is Machine Learning Useful for Macroeconomic Forecasting?" arXiv:2008.12477 .

D'Amour, A., K. Heller, D. Moldovan, et al.. (2022). "Underspecification presents challenges for credibility in modern machine learning." Journal of Machine Learning Research 23, 1–61.

Diebold, F., and R. Mariano. (1995). "Comparing Predictive Accuracy." Journal of Business & Economic Statistics 13, 3, 253–263.

Diebold, F. X.. (2015). "Comparing Predictive Accuracy, Twenty Years Later: A Personal Perspective on the Use and Abuse of Diebold-Mariano Tests." Journal of Business & Economic Statistics 33, 1, 1–1.

Exterkate, P., P.J.F. Groenen, C. Heij, and D. Van Dijk. (2016). "Nonlinear forecasting with many predictors using kernel ridge regression." International Journal of Forecasting 32, 3, 736–753.

Farrell, M. H., T. Liang, and S. Misra. (2021). "Deep neural networks for estimation and inference." Econometrica 89, 1, 181–213.

Faust, J., and J. Wright. (2013). "Forecasting Inflation." In "Handbook of Economic Forecasting," volume 2A, Elsevier.

Fort, S., H. Hu, and B. Lakshminarayanan. (2020). "Deep Ensembles: A Loss Landscape Perspective."

Geirhos, R., J-H. Jacobsen, C. Michaelis, et al.. (2020). "Shortcut learning in deep neural networks." Nature Machine Intelligence 2, 665–673.

Giacomini, R., and B. Rossi. (2010). "Forecast Comparisons in Unstable Environments." Journal of Applied Econometrics 25, 595–620.

Giannone, D., M. Lenza, and G. Primiceri. (2015). "Prior selection for vector autoregressions." Review of Economics and Statistics 97, 2, 436–451.

Glorot, X., and Y. Bengio. (2010). "Understanding the difficulty of training deep feedforward neural networks." Journal of Machine Learning Research - Proceedings Track 9, 249–256.

Goodfellow, I. J., Y. Bengio, and A. Courville (2016). Deep Learning. MIT Press, http://www.deeplearningbook.org.

Gu, S., B. Kelly, and D. Xiu. (2019). "Empirical Asset Pricing via Machine Learning." In "Chicago Booth Research Paper No. 18-04; 31st Australasian Finance and Banking Conference 2018; Yale ICF Working Paper No. 2018-09.", .

Hanin, B., and D. Rolnick. (2018). "How to start training: The effect of initialization and architecture." In "Advances in Neural Information Processing Systems 31," 569–579, Curran Associates, Inc.

Hansen, P. R., A. Lunde, and J. M. Nason. (2011). "The model confidence set." Econometrica 79, 2, 453–497.

Hasenzagl, T., F. Pellegrino, L. Reichlin, and G. Ricco. (2022). "A Model of the Fed's View on Inflation." The Review of Economics and Statistics 104, 4.

Hastie, T., R. Tibshirani, and J. Friedman (2001). The Elements of Statistical Learning. Springer Series in Statistics, New York, NY, USA: Springer New York Inc.

Hauzenberger, N., F. Huber, and K. Klieber. (2022). "Real-time inflation forecasting using non-linear dimension reduction techniques." International Journal of Forecasting, https://doi.org/10.1016/j.ijforecast.2022.03.002 .

He, K., X. Zhang, Ren S., and J. Sun. (2015). "Delving deep into rectifiers: surpassing human-level performance on imagenet classification." In "Proceedings of the IEEE international conference on computer vision.", 1026–1034.

Hinton, G. E., and R. R. Salakhutdinov. (2006). "Reducing the Dimensionality of Data with Neural Networks." Science 313, 5786, 504–507.

Ioffe, S., and C. Szegedy. (2015). "Batch Normalization: Accelerating Deep Network Training by Reducing Internal Covariate Shift." arXiv:1502.03167 .

Izmailov, P., D. Podoprikhin, T. Garipov, D. Vetrov, and A. G. Wilson. (2019). "Averaging Weights Leads to Wider Optima and Better Generalization."

Jain, P., and P. Kar. (2017). "Non-convex Optimization for Machine Learning." Foundations and Trends in Machine Learning 10, 3-4, 142–336.

Kingma, D., and J. Ba. (2015). "Adam: A method for stochastic optimization." In "ICLR," .

Kuan, C-M., and H. White. (1994). "Artificial neural networks: an econometric perspective." Econometric Reviews 13, 1, 1–91.

Ludvigson, S., and S. Ng. (2007). "The empirical risk return relation: A factor analysis approach." Journal of Financial Economics 83, 1, 171–222.

McAdam, P., and P. McNelis. (2005). "Forecasting inflation with thick models and neural networks." Economic Modelling 22, 5, 848–867.

McCracken, M. W., and S. Ng. (2016). "FRED-MD: A monthly database for Macroeconomic Research." Journal of Business & Economic Statistics 34, 4, 574–589.

Medeiros, M. C., G. Vasconcelos, A. Veiga, and E. Zilberman. (2019). "Forecasting Inflation in a Data-Rich Environment: The Benefits of Machine Learning Methods." Journal of Business & Economic Statistics 1–45.

Mullainathan, S., and J. Spiess. (2017). "Machine Learning: An Applied Econometric Approach." Journal of Economic Perspectives 31, 2, 87–106.

Nakamura, E. (2005). "Inflation forecasting using a neural network." Economics Letters 86, 373–378.

Refenes, A.P., and H. White. (1998). "Neural Networks and Financial Economics." International Journal of Forecasting 17, 347–495.

Schmidt-Hieber, J. (2020). "Nonparametric regression using deep neural networks with ReLU activation function." The Annals of Statistics 48, 4, 1875–1897.

Sermpinis, G., C. Stasinakis, K. Theofilatos, and A. Karathanasopoulos. (2014). "Inflation and Unemployment Forecasting with Genetic Support Vector Regression." Journal of Forecasting 33, 471–487.

Stock, J. H., and M. W. Watson. (1999). "Forecasting Inflation." Journal of Monetary Economics 44, 293–335.

Stock, J. H., and M. W. Watson. (2002). "Macroeconomic forecasting with diffusion indexes." Journal of Business & Economic Statistics 20, 147–162.

Stock, J. H., and M. W. Watson. (2007). "Why Has U.S. Inflation Become Harder to Forecast?" Journal of Money, Credit and Banking. 39, 7, 1849–1849.

Stock, J. H., and M. W. Watson. (2009). "Phillips Curve Inflation Forecasts." In "Fuhrer J, Kodrzycki Y, Little J, Olivei G Understanding Inflation and the Implications for Monetary Policy.", 99–202, Cambridge: MIT Press.

Varian, H. R. (2014). "Big data: New tricks for econometrics." The Journal of Economic Perspectives 28, 2, 3–27.

Verstyuk, S.. (2020). "Modeling multivariate time series in economics: From auto-regressions to recurrent neural networks." Available at SSRN 3589337 .

Wilson, A. G., and P. Izmailov. (2022). "Bayesian Deep Learning and a Probabilistic Perspective of Generalization."

Supplementary Materials:
Predicting Inflation with Recurrent Neural Networks

Table of Contents

A Data description

Table S1: Data description

The table describes the data used in the empirical analysis, collected from the FRED monthly database using the October-2019 vintage. I follow McCracken and Ng (2016) and divide the series into eight economic groups. The column Tcode refers to the transformation applied to each series x_t, where (1) no transformation, (2) Δx_t, (3) $\Delta^2 x_t$, (4) $log(x_t)$, (5) $\Delta log(x_t)$, (6) $\Delta^2 log(x_t)$, (7) $\Delta(x_t/x_{t-1} - 1.0)$. The comparable series in Global Insight is given in the column GSI. Percentage of missing values with respect to the full sample (Jan-59 to Oct-19) is included in the last column.

	Tcode	Fred mnemonics	Description	GSI	GSI: description	Missing (%)
Group 1: Output and income						
1	5	RPI	Real Personal Income	M_14386177	PI	
2	5	W875RX1	Real personal income ex transfer receipts	M_145256755	PI less transfers	
3	5	INDPRO	IP Index	M_116460980	IP: total	
4	5	IPFPNSS	IP: Final Products and Nonindustrial Supplies	M_116460981	IP: products	
5	5	IPFINAL	IP: Final Products (Market Group)	M_116461268	IP: final prod	
6	5	IPCONGD	IP: Consumer Goods	M_116460982	IP: cons gds	
7	5	IPDCONGD	IP: Durable Consumer Goods	M_116460983	IP: cons dble	
8	5	IPNCONGD	IP: Nondurable Consumer Goods	M_116460988	IP: cons nondble	
9	5	IPBUSEQ	IP: Business Equipment	M_116460995	IP: bus eqpt	
10	5	IPMAT	IP: Materials	M_116461002	IP: matls	
11	5	IPDMAT	IP: Durable Materials	M_116461004	IP: dble matls	
12	5	IPNMAT	IP: Nondurable Materials	M_116461008	IP: nondble matls	
13	5	IPMANSICS	IP: Manufacturing (SIC)	M_116461013	IP: mfg	
14	5	IPB51222s	IP: Residential Utilities	M_116461276	IP: res util	
15	5	IPFUELS	IP: Fuels	M_116461275	IP: fuels	
16	2	CUMFNS	Capacity Utilization: Manufacturing	M_116461602	Cap util	
Group 2: Labor market						
17	2	HWI	Help-Wanted Index for United States		Help wanted indx	0.14

Continued on next page

Table S1 – *Continued*

	Tcode	Fred mnemonics	Description	GSI	GSI: description	Missing (%)
18	2	HWIURATIO	Ratio of Help Wanted/No. Unemployed	M_110156531	Help wanted/unemp	0.14
19	5	CLF16OV	Civilian Labor Force	M_110156467	Emp CPS total	
20	5	CE16OV	Civilian Employment	M_110156498	Emp CPS nonag	
21	2	UNRATE	Civilian Unemployment Rate	M_110156541	U: all	
22	2	UEMPMEAN	Average Duration of Unemployment (Weeks)	M_110156528	U: mean duration	
23	5	UEMPLT5	Civilians Unemployed - Less Than 5 Weeks	M_110156527	U < 5 wks	
24	5	UEMP5TO14	Civilians Unemployed for 41760 Weeks	M_110156523	U 41760 wks	
25	5	UEMP15OV	Civilians Unemployed - 15 Weeks & Over	M_110156524	U 15+ wks	
26	5	UEMP15T26	Civilians Unemployed for 15-26 Weeks	M_110156525	U 15-26 wks	
27	5	UEMP27OV	Civilians Unemployed for 27 Weeks and Over	M_110156526	U 27+ wks	
28	5	CLAIMSx	Initial Claims	M_15186204	UI claims	
29	5	PAYEMS	All Employees: Total nonfarm	M_123109146	Emp: total	
30	5	USGOOD	All Employees: Goods-Producing Industries	M_123109172	Emp: gds prod	
31	5	CES1021000001	All Employees: Mining and Logging: Mining	M_123109244	Emp: mining	
32	5	USCONS	All Employees: Construction	M_123109331	Emp: const	
33	5	MANEMP	All Employees: Manufacturing	M_123109542	Emp: mfg	
34	5	DMANEMP	All Employees: Durable goods	M_123109573	Emp: dble gds	
35	5	NDMANEMP	All Employees: Nondurable goods	M_123110741	Emp: nondbles	
36	5	SRVPRD	All Employees: Service-Providing Industries	M_123109193	Emp: services	
37	5	USTPU	All Employees: Trade, Transportation & Utilities	M_123111543	Emp: TTU	
38	5	USWTRADE	All Employees: Wholesale Trade	M_123111563	Emp: wholesale	
39	5	USTRADE	All Employees: Retail Trade	M_123111867	Emp: retail	
40	5	USFIRE	All Employees: Financial Activities	M_123112777	Emp: FIRE	
41	5	USGOVT	All Employees: Government	M_123114411	Emp: Govt	
42	1	CES0600000007	Avg Weekly Hours : Goods-Producing	M_140687274	Avg hrs	
43	2	AWOTMAN	Avg Weekly Overtime Hours : Manufacturing	M_123109554	Overtime: mfg	

Continued on next page

Table S1 – *Continued*

	Tcode	Fred mnemonics	Description	GSI	GSI: description	Missing (%)
44	1	AWHMAN	Avg Weekly Hours : Manufacturing	M_14386098	Avg hrs: mfg	
45	6	CES0600000008	Avg Hourly Earnings : Goods-Producing	M_123109182	AHE: goods	
46	6	CES2000000008	Avg Hourly Earnings : Construction	M_123109341	AHE: const	
47	6	CES3000000008	Avg Hourly Earnings : Manufacturing	M_123109552	AHE: mfg	
Group 3: Housing						
48	4	HOUST	Housing Starts: Total New Privately Owned	M_110155536	Starts: nonfarm	
49	4	HOUSTNE	Housing Starts, Northeast	M_110155538	Starts: NE	
50	4	HOUSTMW	Housing Starts, Midwest	M_110155537	Starts: MW	
51	4	HOUSTS	Housing Starts, South	M_110155543	Starts: South	
52	4	HOUSTW	Housing Starts, West	M_110155544	Starts: West	
53	4	PERMIT	New Private Housing Permits (SAAR)	M_110155532	BP: total	1.64
54	4	PERMITNE	New Private Housing Permits, Northeast (SAAR)	M_110155531	BP: NE	1.64
55	4	PERMITMW	New Private Housing Permits, Midwest (SAAR)	M_110155530	BP: MW	1.64
56	4	PERMITS	New Private Housing Permits, South (SAAR)	M_110155533	BP: South	1.64
57	4	PERMITW	New Private Housing Permits, West (SAAR)	M_110155534	BP: West	1.64
Group 4: Consumption, orders and inventories						
58	5	DPCERA3M086SBEA	Real personal consumption expenditures	M_123008274	Real Consumption	
59	5	CMRMTSPLx	Real Manu. and Trade Industries Sales	M_110156998	M&T sales	0.14
60	5	RETAILx	Retail and Food Services Sales	M_130439509	Retail sales	
61	5	ACOGNO	New Orders for Consumer Goods	M_14385863	Orders: cons gds	54.52
62	5	AMDMNOx	New Orders for Durable Goods	M_14386110	Orders: dble gds	
63	5	ANDENOx	New Orders for Nondefense Capital Goods	M_178554409	Orders: cap gds	14.93
64	5	AMDMUOx	Unfilled Orders for Durable Goods	M_14385946	Unf orders: dble	
65	5	BUSINVx	Total Business Inventories	M_15192014	M&T invent	0.14
66	2	ISRATIOx	Total Business: Inventories to Sales Ratio	M_15191529	M&T invent/sales	0.14
67	2	UMCSENTx	Consumer Sentiment Index	hhsntn	Consumer expect	21.10

Continued on next page

Table S1 – *Continued*

	Tcode	Fred mnemonics	Description	GSI	GSI: description	Missing (%)
Group 5: Money and credit						
68	6	M1SL	M1 Money Stock	M_110154984	M1	
69	6	M2SL	M2 Money Stock	M_110154985	M2	
70	5	M2REAL	Real M2 Money Stock	M_110154985	M2 (real)	
71	6	BOGMBASE	Monetary Base	M_110154995	MB	
72	6	TOTRESNS	Total Reserves of Depository Institutions	M_110155011	Reserves tot	
73	7	NONBORRES	Reserves Of Depository Institutions	M_110155009	Reserves nonbor	
74	6	BUSLOANS	Commercial and Industrial Loans	BUSLOANS	C&I loan plus	
75	6	REALLN	Real Estate Loans at All Commercial Banks	BUSLOANS	DC&I loans	
76	6	NONREVSL	Total Nonrevolving Credit	M_110154564	Cons credit	0.14
77	2	CONSPI	Nonrevolving consumer credit to Personal Income	M_110154569	Inst cred/PI	0.14
78	6	MZMSL	MZM Money Stock	N.A.	N.A.	
79	6	DTCOLNVHFNM	Consumer Motor Vehicle Loans Outstanding	N.A.	N.A.	0.14
80	6	DTCTHFNM	Total Consumer Loans and Leases Outstanding	N.A.	N.A.	0.14
81	6	INVEST	Securities in Bank Credit at All Commercial Banks	N.A.	N.A.	
Group 6: Interest and exchange rates						
82	2	FEDFUNDS	Effective Federal Funds Rate	M_110155157	Fed Funds	
83	2	CP3Mx	3-Month AA Financial Commercial Paper Rate	CPF3M	Comm paper	
84	2	TB3MS	3-Month Treasury Bill:	M_110155165	3 T-bill	
85	2	TB6MS	6-Month Treasury Bill:	M_110155166	6 T-bill	
86	2	GS1	1-Year Treasury Rate	M_110155168	1 T-bond	
87	2	GS5	5-Year Treasury Rate	M_110155174	5 T-bond	
88	2	GS10	10-Year Treasury Rate	M_110155169	10 T-bond	
89	2	AAA	Moody's Seasoned Aaa Corporate Bond Yield		Aaa bond	
90	2	BAA	Moody's Seasoned Baa Corporate Bond Yield		Baa bond	
91	1	COMPAPFFx	3-Month Commercial Paper Minus FEDFUNDS		CP-FF spread	

Continued on next page

Table S1 – *Continued*

	Tcode	Fred mnemonics	Description	GSI	GSI: description	Missing (%)
92	1	TB3SMFFM	3-Month Treasury C Minus FEDFUNDS		3 mo-FF spread	
93	1	TB6SMFFM	6-Month Treasury C Minus FEDFUNDS		6 mo-FF spread	
94	1	T1YFFM	1-Year Treasury C Minus FEDFUNDS		1 yr-FF spread	
95	1	T5YFFM	5-Year Treasury C Minus FEDFUNDS		5 yr-FF spread	
96	1	T10YFFM	10-Year Treasury C Minus FEDFUNDS		10 yr-FF spread	
97	1	AAAFFM	Moody's Aaa Corporate Bond Minus FEDFUNDS		Aaa-FF spread	
98	1	BAAFFM	Moody's Baa Corporate Bond Minus FEDFUNDS		Baa-FF spread	
99	5	TWEXAFEGSMTHx	Trade Weighted U.S. Dollar Index		Ex rate: avg	23.01
100	5	EXSZUSx	Switzerland / U.S. Foreign Exchange Rate	M_110154768	Ex rate: Switz	
101	5	EXJPUSx	Japan / U.S. Foreign Exchange Rate	M_110154755	Ex rate: Japan	
102	5	EXUSUKx	U.S. / U.K. Foreign Exchange Rate	M_110154772	Ex rate: UK	
103	5	EXCAUSx	Canada / U.S. Foreign Exchange Rate	M_110154744	EX rate: Canada	
Group 7: Prices						
104	6	WPSFD49207	PPI: Finished Goods	M110157517	PPI: fin gds	
105	6	WPSFD49502	PPI: Finished Consumer Goods	M110157508	PPI: cons gds	
106	6	WPSID61	PPI: Intermediate Materials	M_110157527	PPI: int matls	
107	6	WPSID62	PPI: Crude Materials	M_110157500	PPI: crude matls	
108	6	OILPRICEx	Crude Oil, spliced WTI and Cushing	M_110157273	Spot market price	
109	6	PPICMM	PPI: Metals and metal products:	M_110157335	PPI: nonferrous	
110	5	CPIAUCSL	CPI : All Items	M_110157323	CPI-U: all	
111	6	CPIAPPSL	CPI : Apparel	M_110157299	CPI-U: apparel	
112	6	CPITRNSL	CPI : Transportation	M_110157302	CPI-U: transp	
113	6	CPIMEDSL	CPI : Medical Care	M_110157304	CPI-U: medical	
114	6	CUSR0000SAC	CPI : Commodities	M_110157314	CPI-U: comm.	
115	6	CUSR0000SAD	CPI : Durables	M_110157315	CPI-U: dbles	
116	6	CUSR0000SAS	CPI : Services	M_110157325	CPI-U: services	

Continued on next page

Table S1 – *Continued*

	Tcode	Fred mnemonics	Description	GSI	GSI: description	Missing (%)
117	6	CPIULFSL	CPI : All Items Less Food	M_110157328	CPI-U: ex food	
118	6	CUSR0000SA0L2	CPI : All items less shelter	M_110157329	CPI-U: ex shelter	
119	6	CUSR0000SA0L5	CPI : All items less medical care	M_110157330	CPI-U: ex med	
120	5	PCEPI	Personal Cons. Expend.: Chain Index	gmdc	PCE defl	
121	6	DDURRG3M086SBEA	Personal Cons. Exp: Durable goods	gmdcd	PCE defl: dlbes	
122	6	DNDGRG3M086SBEA	Personal Cons. Exp: Nondurable goods	gmdcn	PCE defl: nondble	
123	6	DSERRG3M086SBEA	Personal Cons. Exp: Services	gmdcs	PCE defl: service	
Group 8: Stock market						
124	5	S&P 500	S&P's Common Stock Price Index: Composite	M_110155044	S&P 500	
125	5	S&P: indust	S&P's Common Stock Price Index: Industrials	M_110155047	S&P: indust	
126	2	S&P div yield	S&P's Composite Common Stock: Dividend Yield		S&P div yield	0.14
127	5	S&P PE ratio	S&P's Composite Common Stock: Price-Earnings Ratio		S&P PE ratio	
128	1	VXOCLSx	VXO			5.75

B On recurrent neural networks

The internal memory of a plain recurrent neural net (RNN) can be described as

$$\begin{aligned} f_{t|L} &= \Gamma(w' z_t + u' f_{t-1|L} + b) \\ f_{0|L} &= 0, \end{aligned} \tag{S1}$$

with parameters $(w, u, b)'$, where $w \in \mathbb{R}^{N \times p}$, $u \in \mathbb{R}^{p \times p}$ and $b \in \mathbb{R}^{p \times 1}$.[9] The final prediction of the RNN is $G(x_t; \Theta_h) = g\Big(f_{t|L}\Big)$, where g is a linear function. Common candidates for Γ are the sigmoid and tanh functions, and is applied element-wise.

The drawback of traditional RNNs is that they usually suffer from vanishing gradients that compromises the estimation process through a slow rate of improvement. Suppose that we seek to estimate an RNN with number of lags L. In brief terms, the estimation of the RNN involves computing the gradient of the loss function with respect to the parameters, which implies evaluating the gradient at every time step within sequences of observations of length L. If the parameters are significantly small (usually they are close to zero), the higher L, the smaller the contribution of observations sufficiently back in time, given the multiplicative effect of the chain rule and the fact that the derivative of the activation function is bounded by 1 (supposing the commonly used tanh or sigmoid functions). In other words, the model will not properly estimate long-term dependencies because the estimation process is compromised for sufficiently long sequences.[10]

The RNN with long-short term memory units, i.e. the LSTM model, solves this problem by avoiding the gradients to be too small, which is key to explaining the long-memory feature usually attributed to LSTMs. The intuition behind this process relies on the existence of a cell state that turns out to be more stable than its counterpart in the traditional RNN, stabilizing the gradients as a consequence. This stability comes from the additive nature of the cell state, as well as the presence of filters that control the flow of information. These features together ensure suitable values for the gradient. For instance, if information from time step l shouldn't be forgotten to predict y_{t+h}, the parameters of specific filters are estimated accordingly so that the gradient at

[9] In this example, and throughout the paper, I assume an RNN with an architecture *many-to-one*, where at each time step the network receives the inputs, updates the internal memory, and only delivers the output after all lags $l = 1, ..., L$ have been processed through the recursion equation. Other variations exist, such as the specification *many-to-many*, in which the network delivers an output at each time step.

[10] In practice, the vanishing gradients problem may also occur in significantly deep feed-forward networks. The use of the *ReLu* activation function in these cases helps preventing the problem because its derivative is either 0 or 1.

the l-time step is sufficiently large to account for this information when updating the model parameters. Intuitively, this mechanism allows the information to effectively flow across time periods. For a more thorough description of RNNs, see Goodfellow et al. (2016).

C On the estimation of neural networks

The parameters of neural network models are estimated by minimizing a loss function between the fitted and actual values over the in-sample period. In this application I use the mean squared error loss as specified in equation (2). Given that the function G is nonlinear with respect to the covariates x_t, the problem of minimizing the loss usually translates into optimizing a non-convex function. In these cases, iterative algorithms are more suitable than the classic optimization procedures applied to convex functions because of their properties that enforce the algorithm to rapidly converge to optima (Jain and Kar, 2017). The literature on neural networks usually applies gradient descent as an optimization method. Gradient descent is based on the property that, to minimize a given function $\mathcal{L}$, one needs to move in the direction of the negative gradient, -$\Delta_\Theta \mathcal{L}(\Theta)$. The parameters are then updated iteratively, such that $\Theta_i = \Theta_{i-1} - \alpha \Delta_\Theta \mathcal{L}(\Theta_{i-1})$, where α is the learning rate, determining the size of the step, and i is the iteration. In this study, I apply an extension of the gradient descent, called Adam optimization algorithm (Kingma and Ba, 2015), that features an adaptive learning rate.

The computation of the gradient may involve a single, random picked observation (stochastic gradient descent), a sub-group of observations (minibatch), or even all available observations (batch gradient descent). For the purpose of this analysis, the number of observations to be included, called batch size, is defined by grid search. Another important concept in machine learning is an epoch, defined as the number of passes of all observations through the algorithm, and not to be confounded with the number of iterations. At each time the gradient is computed, the algorithm updates the parameters, what defines an iteration. Hence, for the case of batch gradient descent the number of epochs coincides with the number of iterations. However for both stochastic gradient descent and minibatch methods, the number of iterations exceeds the number of epochs. The ultimate number of epochs is a hyperparameter selected by grid search.

The estimation process of neural networks, based on incremental updates of the parameters, means that the choice of the initial parameters is an important one. First, assigning equal weights to different nodes implies that they account for the same information and are therefore redundant.

Random initialization is popular because it breaks the symmetry in the network. Second, one should avoid imposing too high or too low initial weight values in order to prevent the vanishing (or exploding) gradient problem, mentioned in Section B. Modern approaches to parameter initialization rely on the idea that the variance of the activations (output of nodes) should be similar across layers (Hanin and Rolnick, 2018). This literature suggests that parameters should therefore be randomly drawn from some zero-centered distribution with a specified variance, while biases are usually initialized with zeros. Common approaches are the Xavier, Glorot and He initializations (Glorot and Bengio, 2010, He et al., 2015). This application considers the Glorot initialization, in which initial weights are drawn from a specific uniform distribution.[11]

The non-convexity usually encountered in neural networks tends to increase the sensitivity of the learning algorithm to initial values. This means that in practice the model delivers a slightly different prediction every time it is re-estimated, given the random initialization. A common solution adopted by the empirical literature is to repeat the estimation a (large) number of times and average out the predictions, which significantly reduces the variance of the prediction and consequently the uncertainty around initial values. Section 7 studies how forecasts compare across models with different initializations and with the ensemble prediction in the context of the present empirical exercise.

D Model specification

The cross-validation process is split into two stages. Stage 1 focuses on hyperparameters specific to the model's architecture, while stage 2 selects the hyperparameters related to the optimization procedure. For example, the number of nodes in the network would be selected in stage 1, while the batch size in stage 2. This method shrinks significantly the computational time compared to the option of selecting all hyperparameters at once. Moreover, previous tests (not reported) indicated that the relative performance of the models are not very sensitive to changes in the number of epochs or batch size. The grid search around these hyperparameters is nonetheless performed for robustness purposes in stage 2. I henceforth refer to "specification" as a particular selection of a set of hyperparameters.

During stage 1, I follow a step-by-step procedure: the FF-cpi and FF-pool models are estimated first, followed by the LSTM-pool and LSTM-all models. As explained below, the cross-validation

[11] Glorot initialization: $W \sim U\left[-\frac{\sqrt{6}}{\sqrt{n_q+n_{q+1}}}, \frac{\sqrt{6}}{\sqrt{n_q+n_{q+1}}}\right]$, where n_q is the number of input units to layer q.

on the FF-LSTM model only occurs in stage 2. Both FF-cpi and FF-pool are estimated over 64 different specifications, where I let vary the number of lags, the number of nodes in the feed-forward layer(s) and the number of hidden layers in the network, as indicated in Table S2.

Second, I use the optimal selection of number of nodes as estimated from the FF models as *fixed* hyperparameters in the cross-validation of the LSTM models (recall that this model also includes a FF section stacked to the LSTM unit). Cross-validation is then performed over 32 different specifications for the LSTM models, including the number of lags, the number of hidden layers and the number of factors. Finally, I set as fixed in the FF-LSTM model the optimal specifications selected from the previous steps. More specifically, I set the number of lags L in the feed-forward part of the model as equal to the optimal value from the FF-cpi, and the number of lags L to be included in the LSTM unit as equal to the optimal value from the LSTM-pool model, as well as the optimal values of nodes and hidden states. The reason behind these choices relies on the similarities between the underlying model structures. The strategy of fixing hyperparameters based on optimal values of nested models facilitates the comparison between models and significantly decreases the computational time. Finally, during stage 2, the hyperparameters related to the optimization process are allowed to vary for all models.

Each model specification is evaluated over a so called validation sample. First consider splitting the full sample with T observations between an in-sample period, of size R, and an out-of-sample period, of size P, such that $T = R + P + h - 1$. The in-sample period is further split into two consecutive sets, the training and validation samples. Each specification is then estimated over the training sample and evaluated over the validation sample.[12] The corresponding performance is used to differentiate between specifications.

More specifically, the cross-validation exercise is implemented as follows: (i) split the data into consecutive samples: training, validation (three different lengths) and out-of-sample set, known as test sample in the machine learning jargon;[13] (ii) for each specification, estimate the model over the training sample and predict over the validation sample; (iii) repeat this process 140 times, and compute the average prediction, defined as the series that averages out the predictions of the 140 series at each point in time; (iv) measure the performance of the average prediction over each of the three sections of the validation sample; and (v) choose the specification with

[12] The forecast performance is measured as the root mean squared error.

[13] Choosing the length of each sample can be quite arbitrary and ultimately depends on each application. Here I split the data such that approximately 60% of the total sample is devoted to training only, 20% to validation and 20% to testing. The precise splits are shown in Figure S1.

Figure S1: Illustrative setup of the cross-validation and out-of-sample forecasting

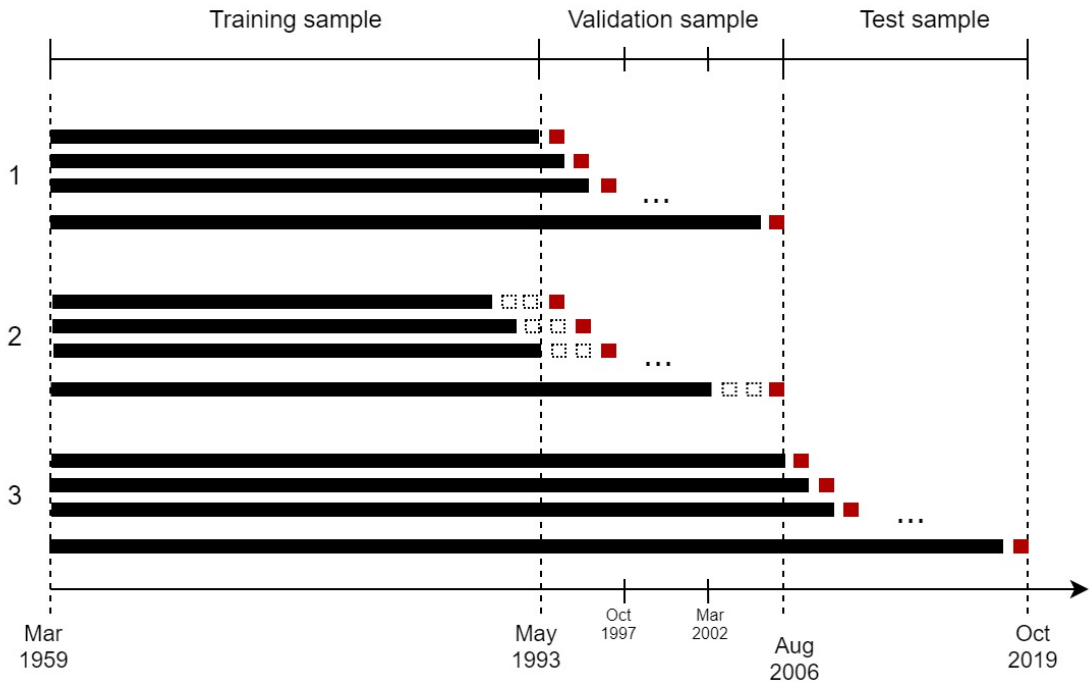

Part 1 (top) depicts the cross-validation over the validation sample for the one-step ahead model. For each specification of hyperparameters, the model is trained over the training sample, and at each step over the validation sample one more data point is added for estimation. The performance over the validation sample is then given by the average performance over three sub-samples: May-1993 to October-1997, May-1993 to March-2002, May-1993 to July-2006. Part 2 (middle) depicts the same cross-validation procedure but for a three-steps ahead model. Note that the predictions cover all data points in the validation set. Finally, part 3 (bottom) illustrates the out-of-sample forecasting for a one-step ahead model, computed for the optimal model selected via cross-validation. The models are re-estimated every 48 months for both the cross-validation and out-of-sample performance.

best average performance over the three sections of the validation sample. The out-of-sample performance is then obtained by evaluating the best specification on unseen data, in which case the final prediction is the average over 1400 different prediction series.[14]

I use a modified version of the more traditional k-fold cross-validation to account for time series characteristics. More specifically, at each time step during cross-validation and out-of-sample performance the estimation set expands by one observation and the prediction is compared with the actual value. By estimating and cross-validating the model on consecutive samples it is possible to avoid the look-ahead bias, since the performance is measured only on future data. In addition, I evaluate each specification over three nested sub-samples of the validation sample, the

[14]The number of iterations for cross-validation is much smaller than the one used for out-of-sample performance as a way of minimizing the computational time given the high number of specifications to estimate. The choice is nonetheless somewhat arbitrary, and the number of repetitions were ultimately set such that it is a multiple of the number of available processors (28).

longest being the full validation set, and choose the model with best average performance over the splits. This is a simple way to add robustness to the analysis, since it minimizes the chances of sample-dependent results. In practice, the choice of the number of splits is quite arbitrary. Here the splits are selected such that the minimum sub-sample size comprises approximately four years of observations.

Table S2: Candidate and optimal values for hyperparameters

	FF-cpi		FF-pool		LSTM-pool		LSTM-all		FF-LSTM	
	Candidates	Optimal	Candidates	Optimal	Candidates	Optimal	Candidates	Optimal	Candidates	Optimal
Stage 1										
lags L	6,12,24,48	24	6,12,24,48	48	6,12,24,48	48	6,12,24,48	48		24, 48
nodes n	16, 32, 64, 128	128	16, 32, 64, 128	128	16, 32, 64, 128	128	16, 32, 64, 128	128		128
layers Q	1,2,3,4	4	1,2,3,4	3	3, 4	4	3, 4	4		4
$f_{t\|L}$-size p					2,4,6,8	2	2,4,6,8	2		2
# parameters		80,513		758,273		51,017		51,097		81,737
Stage 2										
epochs	200,400,600	200	200,400,600	400	200,400,600	400	200,400,600	400	200,400,600	400
batch	128, *max*	128	128, *max*	128	128, *max*	*max*	128, *max*	*max*	128, *max*	128

The table reports the candidate values for each hyperparameter as well as the optimal value selected by cross-validation. The total number of parameters is specific to the CPI target (it is similar for the case of PCE although not exactly the same). The optimal hyperparameters of the FF-cpi and LSTM-pool selected in stage 1 are applied to the FF-LSTM model. Lag L implies that all lags up to L are included in the model. The batch size specified as *max* corresponds to the batch gradient descent method. Not applicable cases are left blank.

Table S3: Hyperparameter values - Small networks

	FF-cpi	FF-pool	LSTM	LSTM-all	FF-LSTM
CPI					
inputs M	10				10
inputs N		118	118	128	118
lags L	24	48	48	48	24, 48
nodes n	4	4	4	4	4
layers Q	4	4	4	4	4
factors p			2	2	2
# parameters	1,029	22,725	1,045	1,125	2,005
PCE					
inputs M	3				3
inputs N		125	125	128	125
lags L	24	48	48	48	24, 48
nodes n	4	4	4	4	4
layers Q	4	4	4	4	4
factors p			2	2	2
# parameters	357	24,069	1,101	1,125	1,389

The table reports the hyperparameters of a set of "smaller" models, where the number of nodes in hidden layers is fixed at 4 and not cross-validated. The other hyperparameters are maintained the same as in table S2. Not applicable cases are left blank.

E Extended results for Section 6.2

Figure S2: Local forecast accuracy and Predictions for CPI inflation - Horizons 3 and 6

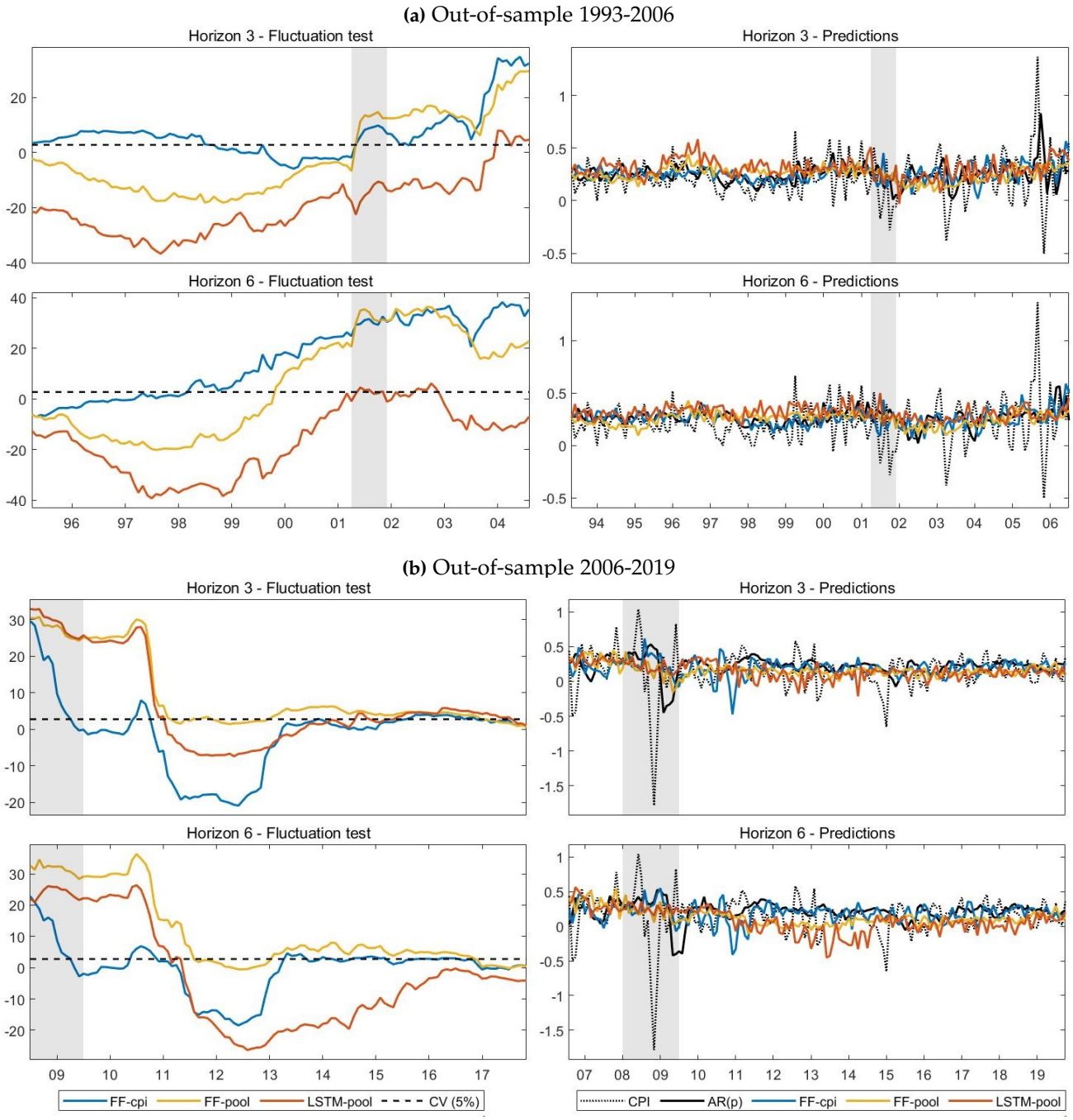

First column: Test statistics according to the Fluctuation Test from Giacomini and Rossi (2010); values above the dashed line indicate that the underlying model presents better forecast accuracy than the $AR(p)$ benchmark over a window of fixed size at the 5% confidence level. Second column: Predictions of selected models; the scale is $100\times$ log differences. Gray areas are NBER recessions.

Table S4: Out-of sample forecast performance for PCE inflation

	1993-2006					2006-2019				
	1	3	6	12	24	1	3	6	12	24
Benchmark models										
UCSV	**1.05**	**1.14**	**1.04**	**1.04**	**0.89****	1.06	0.99	1.02	1.03	**1.05**
Fact	**1.01**	**1.00**	**1.01**	1.10	**1.04**	**0.98**	**1.02**	**1.02**	**1.03**	**1.04**
RF	**0.94***	**1.04**	**1.03**	**0.91*****	**0.89****	**1.01**	**0.87*****	**0.88*****	**0.93*****	**0.90*****
LASSO	**0.97***	**1.04**	**1.06**	**1.03**	**1.01**	**0.93*****	**0.95*****	**0.94*****	**0.93*****	**0.92****
Ridge	**1.00**	**1.10**	1.14	**1.00**	**0.91*****	**1.04**	1.18	1.30	1.17	1.33
ENet	**0.96****	**1.03**	**1.07**	1.03	**1.00**	**0.94*****	**0.92*****	**0.94*****	**0.91*****	**0.90*****
Neural network models										
Large architecture										
FF-cpi	**0.91****	**1.02**	**1.01**	**1.03**	1.22	**1.01**	**0.93*****	**0.92****	**0.94****	**0.95****
FF-pool	**1.04**	**1.12**	**1.10**	**0.96**	**0.98**	**1.01**	**0.84*****	**0.83*****	**0.90****	**0.99**
LSTM-pool	**0.93***	**1.11**	1.21	**0.94***	**0.99**	**1.00**	**0.89****	**0.98**	**0.91****	**0.92****
LSTM-all	**0.93***	**1.09**	1.17	**0.91****	**0.97**	**0.99**	**0.89****	**0.98**	**0.91*****	**0.92****
FF-LSTM	**0.90****	**1.01**	**1.01**	**1.00**	1.11	**1.00**	**0.90*****	**0.90*****	**0.91*****	**0.90*****
Small architecture										
FF-cpi	**0.96**	**1.04**	**1.03**	**1.01**	**1.05**	**1.03**	**0.90*****	**0.90*****	**0.92*****	**0.95****
FF-pool	**1.05**	**1.14**	**1.11**	**0.96***	**0.90*****	**1.06**	**0.86*****	**0.87*****	**0.97**	**1.04**
LSTM-pool	**0.98**	**1.14**	1.25	**0.98**	**0.99**	**1.02**	**0.86*****	**0.88****	**0.90*****	**0.92*****
LSTM-all	**0.98**	**1.13**	1.20	**0.96**	**0.96**	**1.02**	**0.87*****	**0.88****	**0.90*****	**0.92*****
FF-LSTM	**0.92****	**1.04**	**1.04**	**0.93****	**0.89*****	**0.98**	**0.84*****	**0.85*****	**0.86*****	**0.89*****

The table presents the loss ratios with respect to the $AR(p)$ model for horizons $h = 1, 3, 6, 12, 24$ and two OOS periods for models forecasting PCE inflation. The loss function is the RMSE. *, **, *** denote significance of the one-sided DM test at a 10%, 5% and 1% levels respectively. Models retained in the 75% MCS are in bold.

F Extended results for Section 7

Figure S3: Distribution of the CW statistic over different initializations

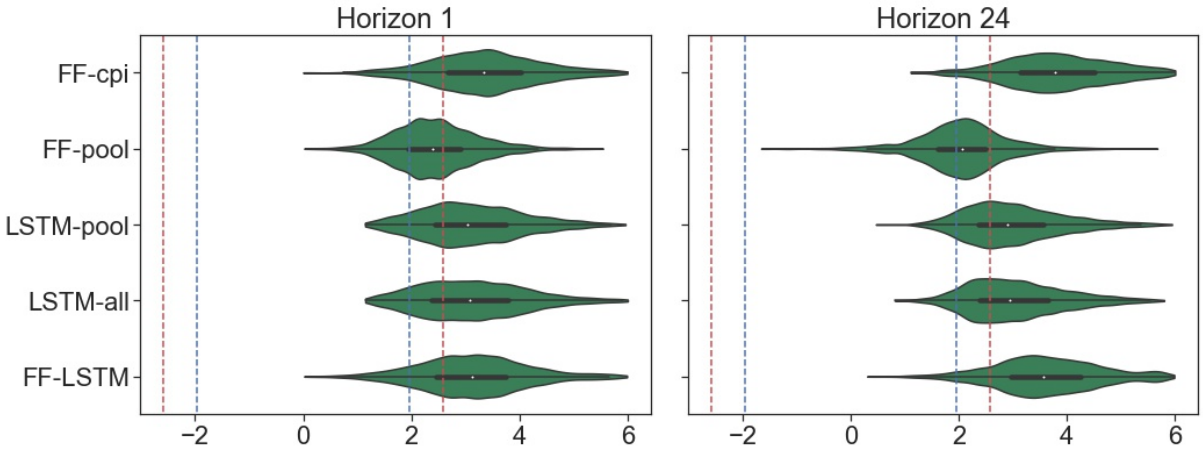

Clark and West (2007) (CW) test statistic $\Delta_{k,h}$, for $k = 1, ..., 1400$ and horizons $h = 1, 24$. Positive values imply better forecast performance of the ensemble prediction over predictions from a particular initialization. Vertical dashed lines are Gaussian critical values at the 5% (blue) and 1% (red) significance levels. Values are truncated at 6 for visualization purposes.

Figure S4: Distribution of the DM statistic over different initializations, Other horizons

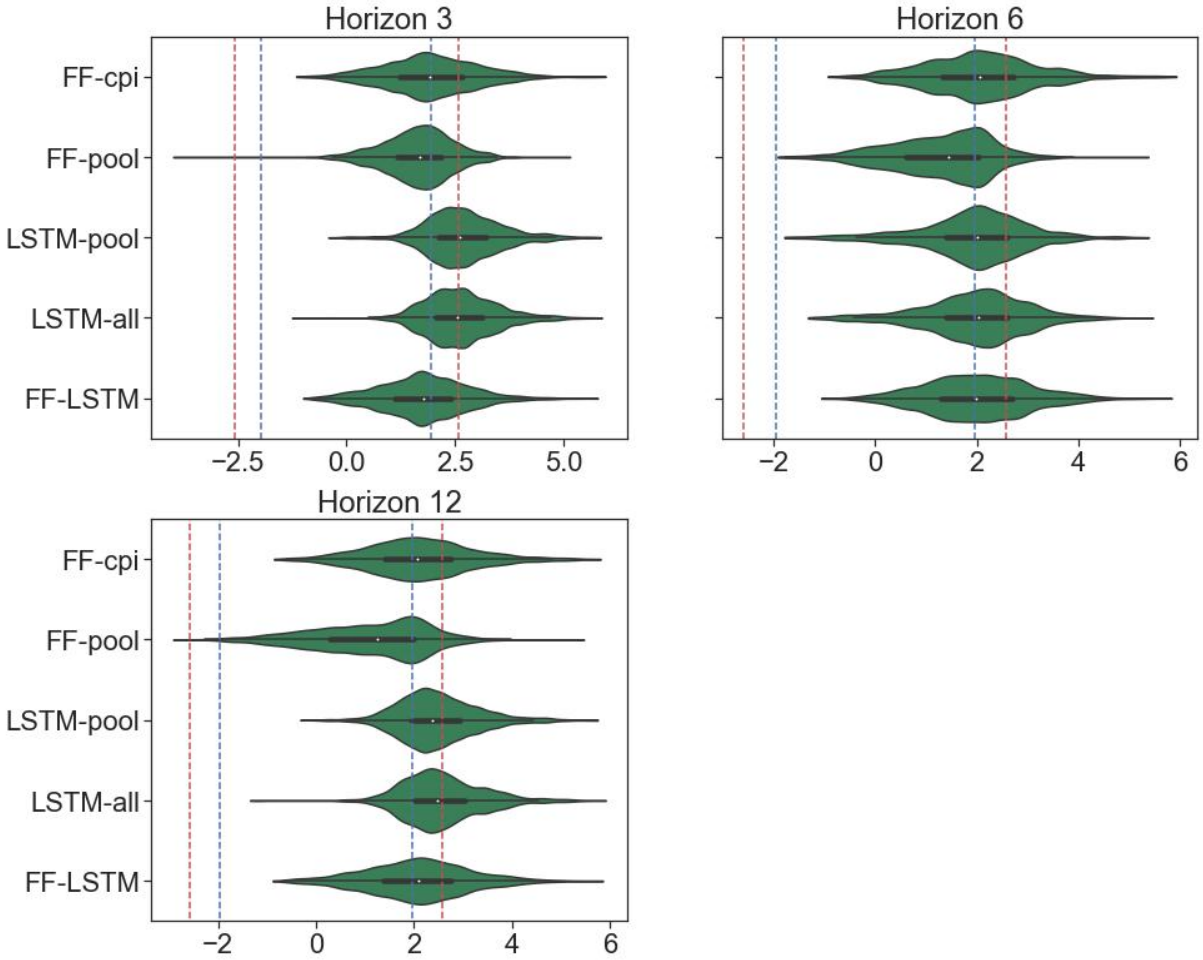

DM test statistic $\Delta_{k,h}$, for $k = 1, ..., 1400$ and horizons $h = 3, 6, 12$. Positive values imply better forecast performance of the ensemble prediction over predictions from a particular initialization. Vertical dashed lines are Gaussian critical values at the 5% (blue) and 1% (red) significance levels. Values are truncated at 6 for visualization purposes.

Figure S5: Distributions of the loss-differential mean and standard deviation over different initializations, FF-cpi and FF-pool models

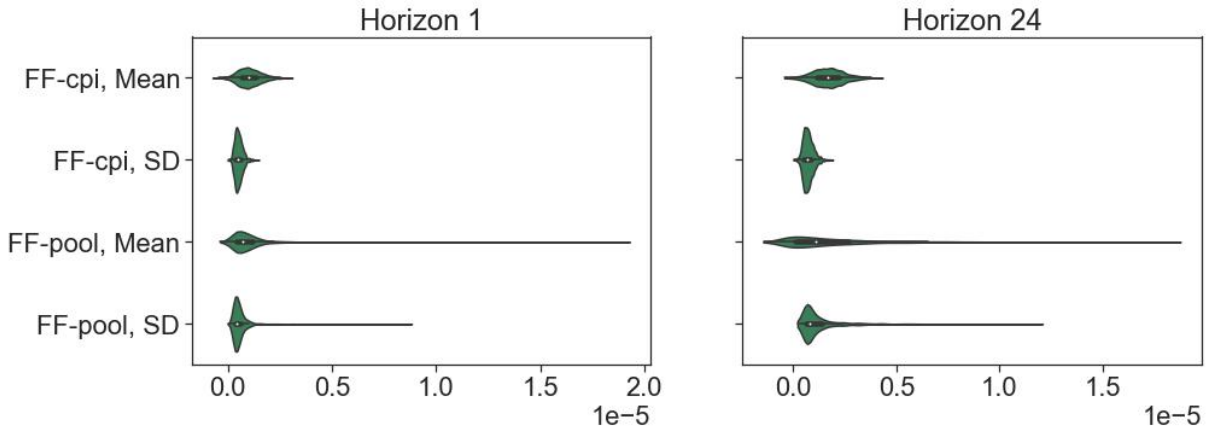

G Benchmark specifications

Consider the inflation series $\pi_t = log(P_t) - log(P_{t-1})$, where P_t is the price index at time t.

G.1 Autoregressive model $AR(p)$

I estimate an autoregressive (AR) model of order p for each horizon, where the h step ahead forecast is given by

$$\widehat{\pi}_{t+h|t} = \widehat{c}_h + \widehat{\Phi}_{1,h}\pi_t + ... + \widehat{\Phi}_{p,h}\pi_{t-(p-1)}.$$

The model is estimated by least squares and p is chosen by Bayesian Information Criterion (BIC), assuming maximum order of 4.

G.2 Unobserved components with stochastic volatility (UCSV)

A second benchmark is the UCSV model from Stock and Watson (2007),

$$\pi_t = \tau_t + e^{h_t/2}\varepsilon_t$$
$$\tau_t = \tau_{t-1} + u_t$$
$$h_t = h_{t-1} + v_t$$

where $\{\varepsilon_t\} \sim iid\mathcal{N}(0,1)$, $\{u_t\} \sim iid\mathcal{N}(0,\omega_\tau^2)$, and $\{v_t\} \sim iid\mathcal{N}(0,\omega_h^2)$. The state processes are initialized with $\tau_1 \sim \mathcal{N}(0, V_\tau)$ and $h_1 \sim \mathcal{N}(0, V_h)$, where $V_\tau = V_h = 0.12$. It is assumed independent inverse-gamma priors for ω_τ^2 and ω_h^2. The model is estimated using Markov Chain Monte Carlo (MCMC) methods, and the h-step ahead forecast is given by

$$\widehat{\pi}_{t+h|t} = \widehat{\tau}_t$$

G.3 Factor-augmented Distributed Lag (FADL) model, the "Factor model"

I specify a FADL(p) model for each horizon h, where the h step ahead forecast is given by

$$\widehat{\pi}_{t+h|t} = \widehat{\beta}_{0,h} + \sum_{i=0}^{p-1}\widehat{\beta}_{i+1,h}\pi_{t-i} + \sum_{j=1}^{r}\sum_{i=0}^{p-1}\widehat{\gamma}_{j,h}f_{j,t-i}.$$

The factors are estimated by principle components applied to the standardized data $\mathcal{Z}$. The number of factors r as well as the number of lags p are jointly selected by BIC, with maximum r

and p set to 4. The model is estimated by least squares.

G.4 Random Forest (RF)

Random forests build on the concept of tree-based regression and classification models, or CART (Breiman et al., 1984; Breiman, 2001). Here I provide a brief overview, and refer to Hastie et al. (2001) for a general introduction of the method.

The idea of tree-based models is essentially to split the predictor space x_t into non-overlapping regions and fit a constant in each one. If the correspondent optimization criterion to choose splits is to minimize the sum of squares residuals, then the constant is simply the average of the target variable in each region. The regions are selected in a greedy manner, in which two regions are first selected out of the original data, then two other regions are selected from each of the first two, and so on. If estimated in the context of random forests, the trees can grown deep, where the minimum number of observations in each region is usually set to a small number.[15]

I consider the predictor set $x_t = (z_t, ..., z_{t-(L-1)}, w_t, ..., w_{t-(L-1)})'$, where L is set to 4. The h step ahead forecast of a single tree with M regions R_m is

$$\widehat{\pi}^{\mathcal{T}}_{t+h|t} = \sum_{m=1}^{M} \widehat{c}_m \, \mathbf{1}\left[x_t \in R_m;\, \Theta^{\mathcal{T}}_h\right],$$

where $\mathbf{1}$ is the indicator function and $\Theta^{\mathcal{T}}_h$ are the parameters of the tree.

Due to their hierarchical nature, trees can be very noisy, as a slight change in predictor values may lead to very different estimates. Forests successfully decrease the variance of tree predictions by combining many (de-correlated) trees in an ensemble fashion. More precisely, the prediction of a forest is

$$\widehat{\pi}_{t+h|t} = \frac{1}{B} \sum_{b=1}^{B} \widehat{\pi}^{\mathcal{T}_b}_{t+h|t},$$

where $\mathcal{T}_b$ is a tree (i) estimated on a (block) bootstrap sample b of the original data, and (ii) considering only a subset $x_{t,b} \in x_t$ of the original predictor set.

[15] I followed default values from the `randomForest` package in `R`, and set the minimum number of observations per region to 5 and the number of trees in the random forest to 500.

G.5 Shrinkage models - LASSO, Ridge and Elastic-net

Shrinkage models yield a h step ahead prediction of the form $\widehat{\pi}_{t+h|t} = \widehat{\beta}_h x_t$, where the coefficients minimize a penalized residual sum of squares,

$$\widehat{\beta}_h = \underset{\beta}{argmin} \sum_{t=1}^{T-h} \left(\pi_{t+h} - \beta_h' x_t\right)^2 + p(\beta_h, \lambda).$$

The tuning parameter $\lambda \geq 0$ controls the amount of shrinkage and is selected by BIC. I consider the predictor set $x_t = (z_t, ..., z_{t-(L-1)}, w_t, ..., w_{t-(L-1)})'$, where L is set to 4, and three variations of the penalty function $p(\beta_h, \lambda)$:

1. LASSO (Least Absolute Shrinkage and Selection Operator), with $p(\beta_h, \lambda) = \lambda \sum_{j=1}^{NT} |\beta_{j,h}|$;
2. Ridge regression, with $p(\beta_h, \lambda) = \lambda \sum_{j=1}^{NT} \beta_{j,h}^2$; and
3. Elastic-net, with $p(\beta_h, \lambda) = \alpha\lambda \sum_{j=1}^{NT} |\beta_{j,h}| + (1-\alpha)\lambda \sum_{j=1}^{NT} \beta_{j,h}^2$. The parameter $\alpha \in [0, 1]$ is selected by BIC.